

Study on Regio- and Diastereoselectivity of the 1,3-Dipolar Cycloaddition Reaction of Azomethine Ylide with 2-(Benzo[d]thiazol-2-yl)-3-(aryl)acrylonitrile: Synthesis, Spectroscopic, and Computational Approach

Essam M. Hussein,* Ziad Moussa, Jabir H. Al-Fahemi, Munirah M. Al-Rooqi, Rami J. Obaid, M. Shaheer Malik, Alaa S. Abd-El-Aziz, and Saleh A. Ahmed*



Cite This: *ACS Omega* 2024, 9, 23802–23821



Read Online

ACCESS |



Metrics & More

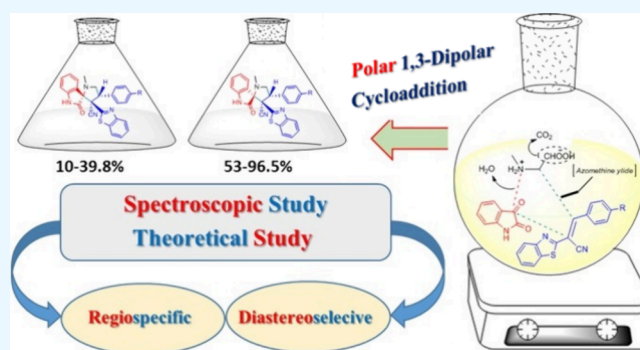


Article Recommendations



Supporting Information

ABSTRACT: An unprecedented and efficient three-component 1,3-dipolar cycloaddition reaction using (*E*)-2-(benzo[d]thiazol-2-yl)-3-(aryl)acrylonitriles **4a–g** and an in situ generated azomethine ylide **3** from isatin and *N*-methylglycine is described. The reaction exhibits exclusive regioselectivity, resulting in the formation of 3'-(benzo[d]thiazol-2-yl)-1'-methyl-2-oxo-4'-(aryl)spiro[indoline-3,2'-pyrrolidine]-3'-carbonitriles regioisomers through *exo/endo* approaches. The diastereoselectivity of the reaction is highly dependent on the substitution pattern of the phenyl ring in dipolarophiles **4a–g**, leading to the formation of *exo/endo*-cycloadducts in varying ratios. To understand the stereoselectivity, the transition state structures were optimized using the TS guess geometry with the QST3-based method. The reaction mechanism and regioselectivity were elucidated by evaluating global and local electrophilicity and nucleophilicity descriptors at the B3LYP/cc-pVTZ level of theory, along with considerations based on the HSAB principle. The analysis of global electron density transfer (GEDT) showed that the reactions are polar and electron density fluxes from azomethine ylide **3** toward dipolarophile **4a–g**. It was found from the molecular electrostatic potential map (MESP) that at the more favorable transition state, approach of reactants locates the oppositely charged regions over each other resulting in attractive forces between the two fragments. The computational results are consistent with the experimental observations, confirming that the reactions proceed through an asynchronous one-step mechanism.



INTRODUCTION

Spirocyclic scaffolds offer significant appeal in drug discovery due to their inherent three-dimensional structure, which facilitates interactions with three-dimensional binding sites more effectively than planar heteroaromatic systems used as ligands. This may explain why a considerable number of spiro compounds constitute a vital class of naturally occurring substances with distinct biological properties, having evolved to interact with proteins.¹ For several decades, the synthesis of pyrrolidine-based heterocycles has garnered significant interest, given their importance as a class of compounds exhibiting distinct biological activities.² Moreover, the incorporation of oxindole derivatives, particularly 3-spirooxindoles conjugated with functionalized pyrrolidines, constitutes a pivotal structural motif found in numerous alkaloids. These compounds serve as compelling targets in organic synthesis because of their diverse range of biological activities.³ Additionally, thiazole and its derivatives hold significant importance in the realms of medicinal and material chemistry. Combining thiazole with

other heterocyclic moieties has demonstrated remarkable biological activities, including antimicrobial properties,⁴ anti-tumor effects,⁵ antispasmodic activity,⁶ and anti-inflammatory potential.⁷

The utilization of 1,3-dipolar cycloaddition involving azomethine ylides (AY) and electron-deficient olefins represents a highly convenient, straightforward, and efficient strategy for constructing highly functionalized pyrrolidine and pyrrolizine rings.⁸ In recent decades, significant advancements have been made in understanding the mechanism and fundamental principles underlying the 1,3-dipolar cycloaddition (32CA) reaction, particularly in terms of selectivity. Numerous studies

Received: February 24, 2024

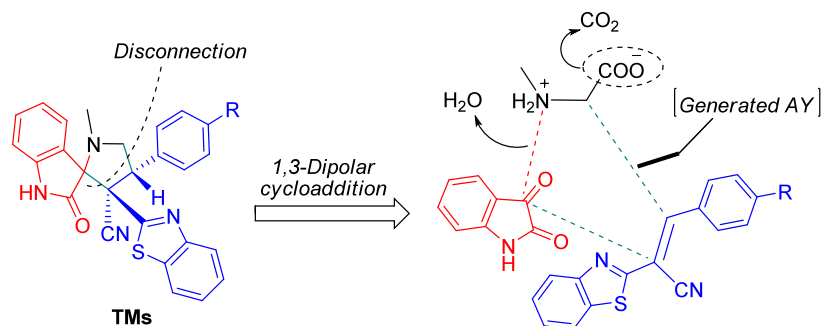
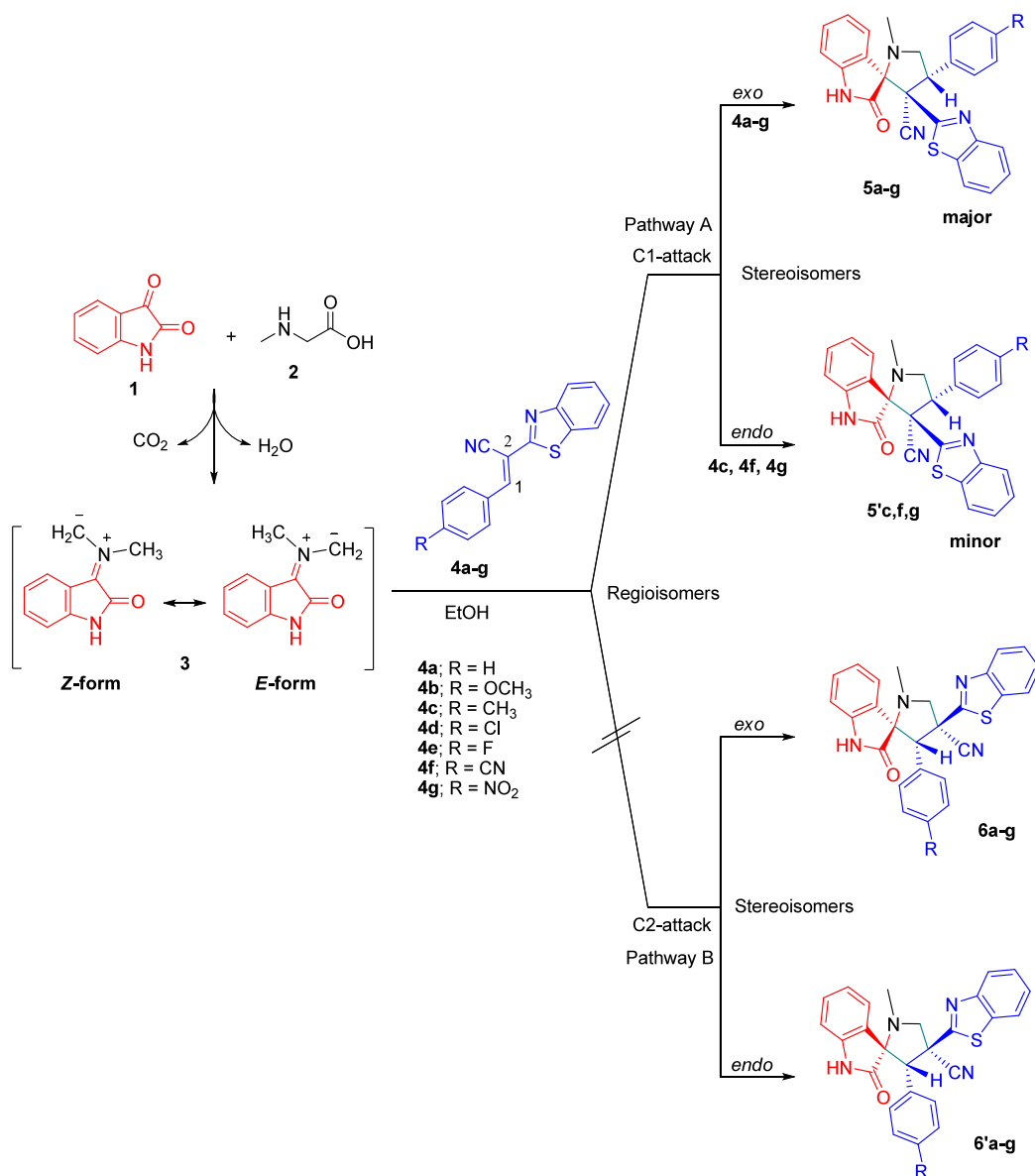
Revised: April 23, 2024

Accepted: May 8, 2024

Published: May 21, 2024



Scheme 1. Retrosynthetic Approach to the Target Spirooxindole-Pyrrolidine-Benzothiazoles TMs

Scheme 2. Synthesis of Diastereomeric Mixture of 3'-(Benzo[*d*]thiazol-2-yl)-1'-methyl-2-oxo-4'-(aryl)spiro[indoline-3,2'-pyrrolidine]-3'-carbonitriles **5** and **5'**

have explored the interplay between theoretical and experimental aspects, contributing to the evolving comprehension of this process. Nevertheless, elucidating the mechanism of 1,3-dipolar cycloadditions remains a persistent challenge. Notably, Domingo made significant contributions to the understanding

of 1,3-dipolar cycloaddition mechanisms by pioneering the use of the molecular electron density theory (MEDT).⁹ According to MEDT, molecular reactivity depends on the ability to change electron density. Thus, reactivity in organic chemistry can be described by a quantum chemical analysis of the changes in

Table 1. 1,3-Dipolar Cycloaddition Reaction of Isatin (1) and *N*-Methylglycine (2) with Dipolarophiles 4a–g

Entry	Reactants	Products	R	Time (h)	Yield (%) ^a	Regioselectivity (%) ^b		Stereoselectivity (%) ^b
						C1:C2 attack		5:5'
1	1 + 2 + 4a	5a	-H	4	55.4	100:0		100:0
2	1 + 2 + 4b	5b	-OCH ₃	5	83.2	100:0		100:0
3	1 + 2 + 4c	5c + 5'c	-CH ₃	4	92.8	100:0		57:43
4	1 + 2 + 4d	5d	-Cl	3	52.7	100:0		100:0
5	1 + 2 + 4e	5e	-F	2	96.5	100:0		100:0
6	1 + 2 + 4f	5f + 5'f	-CN	3	96.2	100:0		68:32
7	1 + 2 + 4g	5g + 5'g	-NO ₂	3	86.4	100:0		88:12

^aCombined yield of isolated cycloadducts. ^bSeparated by column chromatography workup.

electron density and their energies along the reaction pathway.¹⁰ Domingo et al. used this methodology to analyze bond formation along the nonpolar and polar 32CA reactions.¹¹ They show that these reactions follow a *two-stage one-step* mechanism.¹²

As part of our ongoing exploration of 1,3-dipolar cycloaddition reactions,¹³ we present, for the first time, a straightforward and efficient method to access spirooxindole-pyrrolidine-benzothiazole heterocyclic hybrids **TMs**. The synthetic approach involves a one-pot, three-component reaction utilizing a 1,3-dipolar cycloaddition reaction of nonstabilized azomethine ylide, which is generated in situ through the decarboxylative condensation of isatin and *N*-methylglycine, with a series of (*E*)-2-(benzo[*d*]thiazol-2-yl)-3-(aryl)acrylonitriles (Scheme 1).

Theoretical analysis of all possible regio- and stereocycloaddition pathways were carried out by calculating global/local electrophilicity/nucleophilicity reactivity indices and the corresponding transition states (TSs) at the B3LYP/cc-pVTZ level of theory.

RESULTS AND DISCUSSION

Synthetic Approach and Spectroscopic Verification.

The 1,3-dipolar cycloaddition reaction of nonstabilized azomethine ylide **3**, generated in situ via decarboxylative condensation of isatin (**1**) and *N*-methylglycine (**2**), with variously substituted (*E*)-2-(benzo[*d*]thiazol-2-yl)-3-(aryl)acrylonitrile in absolute ethanol afforded a series of novel 3'-(benzo[*d*]thiazol-2-yl)-1'-methyl-2-oxo-4'-(aryl)spiro[indoline-3,2'-pyrrolidine]-3'-carbonitriles in moderate to excellent yields (Scheme 2). Remarkably, the reaction displayed exclusive regioselectivity, yielding one of the two possible regioisomers, and high diastereoselectivity, affording two of the four possible diastereomers (Scheme 2 and Table 1).

The reaction was found to be regiospecific, consistently leading to the formation of a single regioisomer through C1-attack in all instances. Furthermore, it demonstrated high diastereoselectivity at the spirocenter, which depended on the substitution pattern of the phenyl ring in dipolarophiles **4a–g**, resulting in the formation of *exo*-/*endo*-cycloadducts in varying ratios (Table 1). The diastereomeric products displayed distinct retardation factors, allowing for effective separation via column chromatography. In most cases, the *exo*-cycloadduct was obtained as the sole diastereomer, with the exception of dipolarophiles **4c**, **4f**, and **4g** (Table 1, entries 3, 6, and 7), where the *endo*-cycloadduct was obtained as a minor diastereomer.

Consequently, to fully establish the regiochemical and stereochemical outcome of the reaction, extensive one-dimension (¹H-, ¹³C-, ¹³C-DEPT-45/90/135-NMR) and two-dimension homonuclear and heteronuclear correlation NMR

spectrometry techniques were carried out (¹H–¹H-DQF-COSY, ¹H–¹³C-HSQC, ¹H–¹³C-HMBC, ¹H–¹H-NOESY, ¹H–¹H-ROESY) (see the Supporting Information). Using 3'-(benzo[*d*]thiazol-2-yl)-1'-methyl-4'-(4-nitrophenyl)-2-oxospiro[indoline-3,2'-pyrrolidine]-3'-carbonitriles (**5g**) and (**5'g**) as a representative structural models, the relevant spectra used for conclusive regiochemical and stereochemical structural analysis and elucidation are shown in Figures 1 and 2. Although collecting single-crystal X-ray diffraction data would comprise the proper means to determine the regiochemistry and absolute stereochemistry, this was not possible in this case since none of the products could be grown into crystals suitable for X-ray analysis.

Regiochemical Assignment of Cycloadduct (5g). Analysis of the ¹³C (see the Supporting Information, Figure S68), ¹³C-DEPT-45/90 (see the Supporting Information, Figures S69–S70), and ¹³C-DEPT-135 (Figure 1, spectrum b) NMR spectra confirmed the presence of 24 signals (10 aromatic CH's, 7 aromatic quaternary carbons, 1 *N*-methyl, 1 nitrile, 1 carbonyl carbon, 2 quaternary *sp*³-hybridized centers, one methylene, and one methine carbons), which is agreeable with all carbons being magnetically nonequivalent except for C_{2'} and C_{3'} (Figure 1). The oxindoline carbonyl (C₂) appears at δ 174.5 ppm, and the spirocenter carbon (C₃/C_{2'}) of the pyrrolidine ring, which represents a key indicator of a successful annulation reaction, resonates farthest downfield (δ 78.6 ppm) amid all the carbon atoms of this ring which incidentally are the only nuclei exhibiting chemical shifts in the aliphatic region of the carbon spectrum besides the *N*-methyl group. The distinctive peak at δ 46.4 ppm has been attributed to the C_{4'}-H carbon since it is the sole aliphatic signal appearing in the ¹³C-DEPT-90 and was correlated to the most deshielded aliphatic proton signal appearing as a doublet of doublets at δ 5.93 (*J* = 10.2, 6.6 Hz, C_{4'}-H). Meanwhile, the methylene ¹³C_{5'} chemical shift (C_{5'}/δ 56.6 ppm) was clearly identified as the only signal with a negative phase in the ¹³C-DEPT-135 spectrum with its attached diastereotopic protons H_a and H_b appearing as apparent triplet (δ 3.94, *J* = 10.2 Hz, C_{5'}-H_a) and doublet of doublets (δ 3.82, *J* = 9.6, 6.6 Hz, C_{5'}-H_b), respectively. The methylene protons were correlated in the ¹H–¹³C-HSQC-NMR spectrum by two contours to the corresponding C_{5'} carbon (Figure 1, spectrum d). The nonequivalent pyrrolidine protons (C_{4'}-H, C_{5'}-H_a and C_{5'}-H_b) were correlated to the same spin system by ¹H–¹H-DQF-COSY (9-contour square in the aliphatic region, Figure 1, spectrum c), providing irrefutable evidence to support the suggested regiochemistry **5** and disprove the alternative regiochemical outcome **6** where the methylene and methine comprise isolated uncoupled spin systems.

The methine proton of C_{4'}-H (δ 5.93 ppm) shows strong long-range ¹H–¹³C heteronuclear multiple bond correlation

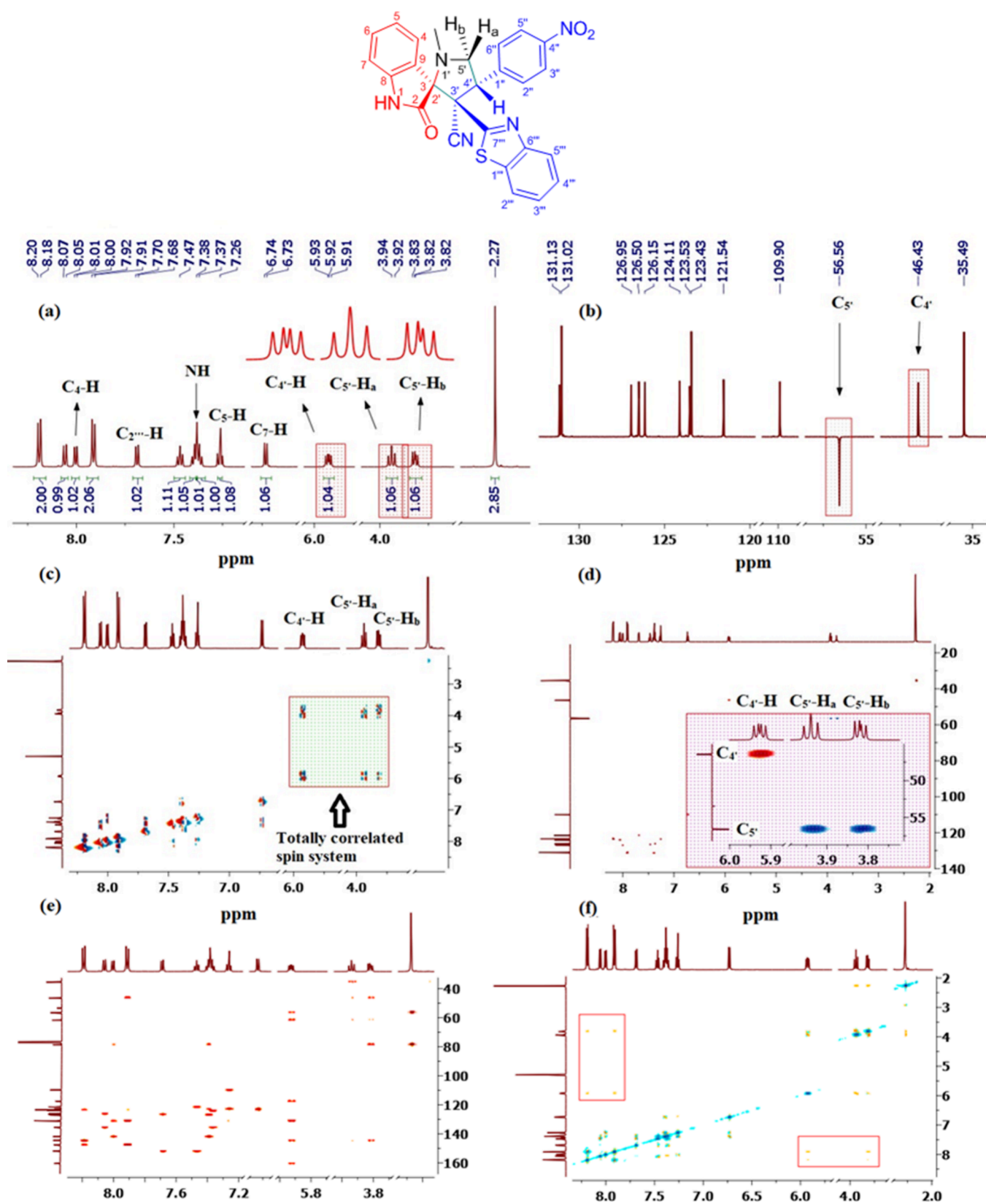


Figure 1. (a) Truncated one dimension and two-dimension NMR spectra of 3'-(benzo[*d*]thiazol-2-yl)-1'-methyl-4'-(4-nitrophenyl)-2-oxospiro[indoline-3,2'-pyrrolidine]-3'-carbonitrile (**5g**) (CDCl₃, 600 MHz): (a) ¹H NMR spectrum; (b) ¹³C-DEPT-135 spectrum, CH's and CH₃'s (positive phase), CH₂'s (negative phase); (c) ¹H-¹H-gDQCOSY-NMR spectrum; (d) ¹H-¹³C-HSQC-NMR spectrum; (e) ¹H-¹³C-gHMBC-NMR spectrum; and (f) ¹H-¹H-ROESY-NMR spectrum.

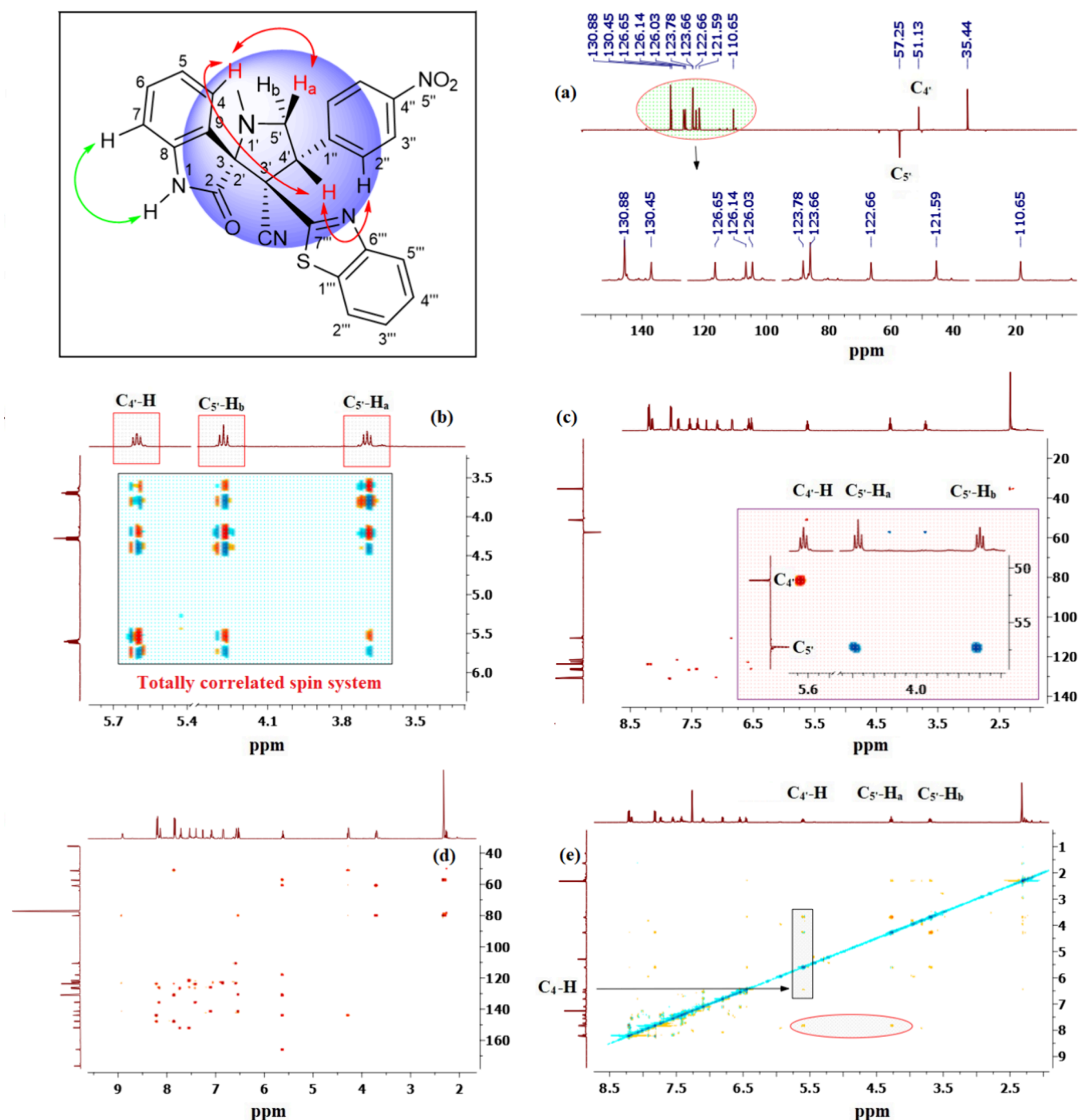


Figure 2. (a) Truncated one dimension and two dimension NMR spectra of 3'-(benzo[*d*]thiazol-2-yl)-1'-methyl-4'-(4-nitrophenyl)-2-oxospiro[indoline-3,2'-pyrrolidine]-3'-carbonitrile (**5g**) (CDCl₃, 600 MHz): (a) ¹³C-DEPT-135 spectrum, CH's and CH₃'s (positive phase), CH₂'s (negative phase); (b) ¹H-¹H-gDQCOSY-NMR spectrum; (c) ¹H-¹³C-HSQC-NMR spectrum; (d) ¹H-¹³C-gHMBC-NMR spectrum; and (e) ¹H-¹H-ROESY-NMR spectrum.

(HMBC) (³J_{CH}) with spirocenter C₃/C₂' (δ 78.6 ppm), benzothiazole C_{7'''} (δ 160.5 ppm), CN (δ 117.5 ppm), and C_{2''} of the 4-nitrophenyl ring (δ 131.0 ppm).

Meanwhile, the methylene protons of C₅-H₂ show strong long-range ¹H-¹³C-HMBC (³J_{CH}) with N₁'-Me (δ 35.5 ppm), spirocenter C₃/C₂', pyrrolidine C₃' (δ 61.7 ppm), and C_{1''} of the 4-nitrophenyl ring (δ 144.6 ppm). The ¹H chemical shifts of the 4-nitrophenyl protons (C_{2''}: δ 7.91; C_{3''}: δ 8.19 ppm) were identified through ¹H-¹H-COSY (4-contour square in the aromatic region, Figure 1, spectrum c), and their respective ¹³C

chemical shifts were verified through correlation contours at δ 131.0 (C_{2''}) and 123.4 (C_{3''}) ppm in the ¹H-¹³C-gHSQC NMR. The ¹³C chemical shift of the remaining C_{4''} (δ 147.6 ppm) was confirmed through the ¹H-¹³C-HMBC cross peak (³J_{CH}) with C_{2''}-H.

Stereochemical Assignment of "exo" Cycloadduct (5g). It was critical to assign all the chemical shifts of the aromatic protons of the benzothiazole and oxindoline rings ahead of attempting any kind of stereochemical analysis and determination. Pleasingly, the -NH group of the oxindoline moiety (δ

7.38 ppm/ ^1H NMR, Figure 1, spectrum a) provided the key entry point that ultimately led to unequivocal determination of the correct stereochemistry for the isolated diastereomer. Specifically, in the ^1H - ^1H -ROESY spectrum (Figure 1, spectrum f) there exists a strong correlation contour between the -NH proton (δ 7.38 ppm) and H-7 (doublet, δ 6.73 ppm), and recognition of the latter triggered the identification of the remaining oxindoline protons in the same spin system and assignment of their relative position on the aromatic ring. Hence, while ^1H - ^1H -COSY correlated H-7 to H-6 (triplet, δ 7.40 ppm), H-6 to H-5 (triplet, δ 7.26 ppm), and H-5 to H-4 (doublet, δ 8.00 ppm), the ^1H - ^{13}C -HSQC correlated the H-4 (δ 8.00/127.0), H-5 (δ 7.26/123.5), H-6 (δ 7.40/131.1), and H-7 (δ 6.73/109.9) to the corresponding ^{13}C chemical shifts. Further strong proof for the preceding assignment order stems from a strong ^1H - ^{13}C -HMBC ($^3J_{\text{CH}}$) correlation of H-4 with spirocenter carbon (C_3/C_2). The remaining two quaternary carbons, C_8 (δ 141.9 ppm) and C_9 (δ 122.8 ppm), were identified through ^1H - ^{13}C -HMBC cross peaks ($^3J_{\text{CH}}$) with C_4 -H/ C_6 -H and C_5 -H/ C_7 -H, respectively. The chemical shifts of the benzothiazole protons and carbons were identified using $\text{H}_{2''}$ as an entry point after recognizing $\text{H}_{2''}$ as the doublet at δ 7.69 ppm based on strong ^1H - ^{13}C -HMBC cross peak ($^3J_{\text{CH}}$) with $\text{N}-\text{C}_{6''}$ (δ 7.69/151.9), which is anticipated to be the most downfield shift of the benzothiazole ring. Thus, while ^1H - ^1H -COSY correlated $\text{H}_{2''}$ to $\text{H}_{3''}$ (triplet, δ 7.37 ppm), $\text{H}_{3''}$ to $\text{H}_{4''}$ (triplet, δ 7.47 ppm), and $\text{H}_{4''}$ to $\text{H}_{5''}$ (doublet, δ 8.06 ppm), ^1H - ^{13}C -HSQC correlated the $\text{H}_{2''}$ (δ 7.69/121.5), $\text{H}_{3''}$ (δ 7.37/126.2), $\text{H}_{4''}$ (δ 7.47/126.5), and $\text{H}_{5''}$ (δ 8.06/124.1) to the corresponding ^{13}C chemical shifts. Additional verification for the foregoing assignment order stems from strong ^1H - ^{13}C -HMBC ($^3J_{\text{CH}}$) correlations of $\text{H}_{4''}$ with $\text{N}-\text{C}_{6''}$ (δ 7.47/151.9) and both $\text{H}_{3''}$ and $\text{H}_{5''}$ with $\text{S}-\text{C}_{1''}$ (δ 8.06/7.37/135.6). The chemical shifts of the 4-nitrophenyl protons and carbons were identified using C_4 -H as an entry point after identifying $\text{H}_{2''}$ as the doublet at δ 7.91 ppm based on strong ^1H - ^{13}C -HMBC (Figure 1, spectrum e) cross peak ($^3J_{\text{CH}}$) of C_4 -H with $\text{C}_{2''}$ (δ 5.93/131.0), where the $\text{C}_{2''}$ chemical shift was correlated in the ^1H - ^{13}C -HSQC (Figure 1, spectrum d) to $\text{H}_{2''}$ (δ 7.91) and $\text{H}_{2''}$ was correlated in the ^1H - ^1H -COSY to $\text{H}_{3''}$ (δ 8.19). The ^{13}C chemical shift of the latter was identified through the ^1H - ^{13}C -HSQC spectrum (δ 123.4). The remaining two quaternary carbons, $\text{C}_{1''}$ (δ 144.6 ppm) and $\text{C}_{4''}$ (δ 147.6 ppm), were identified through ^1H - ^{13}C -HMBC cross peaks ($^3J_{\text{CH}}$) with $\text{C}_{3''}$ -H/ C_5 -H₂ and C_2 -H, respectively. The stereochemistry of the nonequivalent methylene protons of C_5 , H_a (δ 3.94, app t, J = 10.2 Hz) and H_b (δ 3.82, 9.6, 6.6 Hz) was determined relative to C_4 -H based on two very strong cross peaks in the ^1H - ^1H -ROESY spectrum between H_b/C_4 -H and the 4-nitrophenyl- $\text{H}_{2''}$, indicating the close proximity of the latter to H_b and C_4 -H compared to H_a .

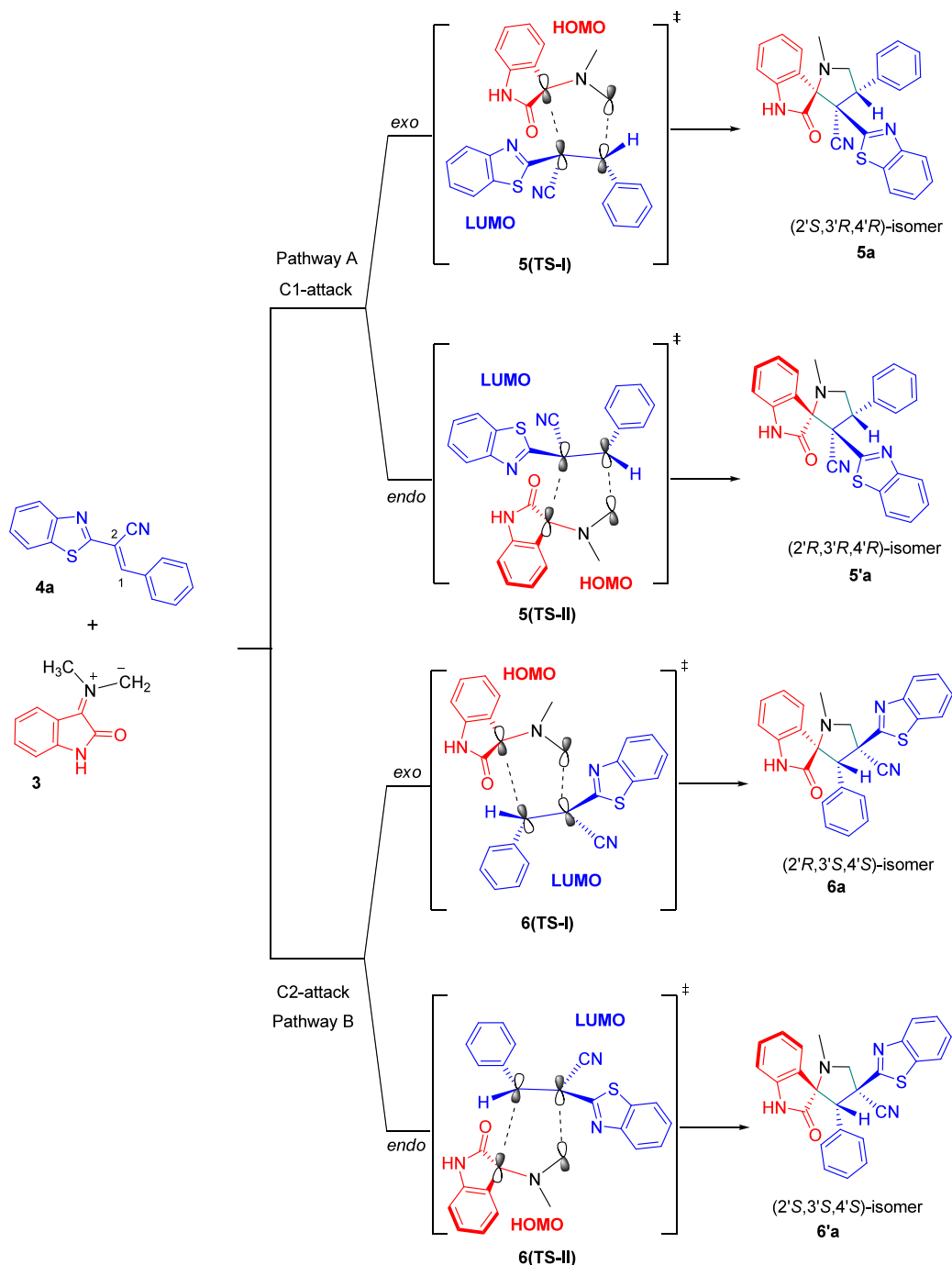
Having assigned the proton and carbon chemical shifts for the benzothiazole, oxindoline, 4-nitrophenyl, and pyrrolidine rings, what remained was to inspect the ^1H - ^1H -ROESY spectrum for any important spatial proximity cross peaks that could be utilized to assign the relative stereochemistry of the three stereogenic centers. As may be anticipated, cycloaddition reactions are inherently diastereoselective and the relative stereochemistry of the two stereogenic centers C_4 and C_3 are predictable based on the initial trans geometry of the dipolarophile, (*E*)-2-(benzo[*d*]thiazol-2-yl)-3-(aryl)-acrylonitrile. Thus, the benzothiazole and 4-nitrophenyl rings are expected to be trans. Indeed the ^1H - ^1H -ROESY spectrum

shows no correlation contours between any of the protons of these two rings, ruling out syn stereochemistry. One, however, still expects the formation of two diastereomeric products due to the creation of a second spirocenter ($\text{C}_{2/3}$) during the process. Notably, the ^1H NMR signals of C_4 -H, C_5 - H_a , and C_4 -H, which incidentally have been previously used in related systems^{13e} to assign the relative stereochemistry of all chiral centers, were most informative and served also herein as key in assigning the relative stereochemistry. Thus, the complete absence of cross peaks between C_4 -H and C_4 -H as well as between C_5 - H_a and C_4 -H indicated a lack of proximity and an anti-relationship of C_4 -H with both, C_5 - H_a and C_4 -H.

Regiochemical Assignment of "endo" Cycloadduct (5'g). Having set up a dependable spectroscopic tactic to identify and correlate all proton and carbon signals for the preceding pure "exo" diastereomer of 3'-(benzo[*d*]thiazol-2-yl)-1'-methyl-4'-(4-nitrophenyl)-2-oxospiro[indoline-3,2'-pyrrolidine]-3'-carbonitrile (5g), regio- and stereochemical analysis of the second isomeric product isolated from the reaction followed a similar strategy. To this end, 1D and 2D NMR spectroscopy were employed to verify the structure obtained from the second fraction of 3'-(benzo[*d*]thiazol-2-yl)-1'-methyl-4'-(4-nitrophenyl)-2-oxospiro[indoline-3,2'-pyrrolidine]-3'-carbonitrile (5'g). The subsequent discussion provides detailed insights and accompanying NMR spectra that lend support to the proposed regio- and stereochemistry of 5'g.

Examination of the ^{13}C -DEPT-135 (Figure 2, spectrum a), ^{13}C (see the Supporting Information, S78), ^{13}C -DEPT-90 (see the Supporting Information, Figure S79) NMR spectra confirmed the presence of 24 signals (10 aromatic CH's, 7 aromatic quaternary carbons, 1 *N*-methyl, 1 nitrile, 1 carbonyl carbon, 2 quaternary sp^3 -hybridized centers, one CH_2 , and one alicyclic methine), which is consistent with all carbon atoms being magnetically nonequivalent except for the 4-nitrophenyl carbons, $\text{C}_{2''}$ and $\text{C}_{3''}$ (Figure 2). The oxindoline carbonyl (C_2) appears at δ 176.4 ppm, and the spirocenter carbon (C_3/C_2) of the pyrrolidine ring, which indicates a successful cyclization reaction, absorbed furthest downfield (δ 80.1 ppm) among all the carbon atoms of this ring which, incidentally, are the only nuclei exhibiting chemical shifts in the aliphatic region of the carbon spectrum besides the *N*-methyl group. The distinctive peak at δ 51.1 ppm has been attributed to the C_4 -H carbon since it is the sole aliphatic signal appearing in the ^{13}C -DEPT-90 and was correlated to the most deshielded aliphatic proton signal appearing as doublet of doublets at δ 5.60 (dd, J = 9.6, 8.4 Hz, 1H, C_4 -H). Meanwhile, the methylene $^{13}\text{C}_{5'}$ chemical shift ($\text{C}_{5'}/\delta$ 57.3 ppm) was clearly recognized as the only signal with a negative phase in the ^{13}C -DEPT-135 spectrum (Figure 2, spectrum a) with its attached nonequivalent diastereotopic protons H_a and H_b appearing as apparent triplet (δ 4.28, J = 10.2 Hz, C_5 - H_b) and doublet of doublets (δ 3.70, J = 9.6, 8.4 Hz, C_5 - H_a), respectively (Figure 2, spectrum c). The methylene protons were correlated in the ^1H - ^{13}C -HSQC-NMR spectrum by two contours to the corresponding C_5 carbon (Figure 2, spectrum c). Strong diamagnetic anisotropic effect caused unexpected large separation between C_5 - H_a and C_5 - H_b . The nonequivalent pyrrolidine protons (C_4 -H, C_5 - H_a , and C_5 - H_b) were traced to the same spin system by ^1H - ^1H -DQF-COSY (9-contour square in the aliphatic region, Figure 2, spectrum b), delivering undisputable evidence to back the suggested regiochemistry 5' and negate the other regiochemical outcome 6' where the methylene and methine comprise isolated uncoupled spin systems. The methine proton of C_4 -H (δ 5.60 ppm) shows

Scheme 3. Regio- and Stereoisomeric Pathways for the 32CA Reaction between Azomethine Ylide 3 and Alkene 4a



strong long-range ^1H - ^{13}C heteronuclear multiple bond correlation (HMBC) ($^3J_{\text{CH}}$) with benzothiazole $\text{C}_{7''}$ (δ 165.7 ppm), CN (δ 118.0 ppm), and $\text{C}_{2''}$ of the 4-nitrophenyl ring (δ 130.9 ppm) as well as HMBC correlation ($^2J_{\text{CH}}$) with $\text{C}_{1''}$ (δ 143.9 ppm), $\text{C}_{3''}$ (δ 60.8 ppm), and $\text{C}_{5''}$ (δ 57.3 ppm). Meanwhile, the methylene protons of $\text{C}_5\text{-H}_2$ show strong long-range ^1H - ^{13}C -HMBC ($^3J_{\text{CH}}$) with $\text{N}_{1''}\text{-Me}$ (δ 35.4 ppm), spirocenter $\text{C}_3/\text{C}_{2'}$ (δ 80.1 ppm), pyrrolidine $\text{C}_{3'}$ (δ 60.8 ppm), and $\text{C}_{1''}$ of the 4-nitrophenyl ring (δ 143.9 ppm) as well as $\text{C}_{4'}$ (δ 51.1 ppm; $^2J_{\text{CH}}$). The ^1H chemical shifts of the 4-nitrophenyl protons ($\text{C}_{2''}$: δ 7.82; $\text{C}_{3''}$: δ 8.21 ppm) were identified through ^1H - ^1H -COSY (4-contour square in the aromatic region, Figure 2, spectrum b), and their respective ^{13}C chemical shifts were

verified through correlation contours at δ 130.9 ($\text{C}_{2''}$) and 122.7 ($\text{C}_{3''}$) ppm in the ^1H - ^{13}C -gHSQC NMR (Figure 2, spectrum c). The ^{13}C chemical shift of the remaining $\text{C}_{4''}$ (δ 147.8 ppm) was confirmed through the ^1H - ^{13}C -HMBC cross peak ($^3J_{\text{CH}}$) with $\text{C}_{2''}\text{-H}$.

Stereochemical Assignment of "endo" Cycloadduct (5'g).

It was crucial to determine all the chemical shifts of the aromatic protons of the benzothiazole and oxindoline rings ahead of attempting any sort of stereochemical analysis and determination. Pleasingly, the $-\text{NH}$ group of the oxindoline moiety (δ 8.07 ppm/ ^1H NMR, see the Supporting Information) provided the key entry point that ultimately led to unequivocal determination of the correct stereochemistry for the isolated

diastereomer. Specifically, in the ^1H – ^1H -ROESY spectrum (Figure 2, spectrum e), there exists a strong correlation contour between the –NH proton (δ 8.07 ppm) and H-7 (doublet, δ 6.81 ppm), and identification of the latter initiated the recognition of the remaining oxindoline protons in the same spin system and assignment of their relative positions on the aromatic ring. Henceforth, while ^1H – ^1H -COSY (Figure 2, spectrum b) correlated H-7 to H-6 (triplet, δ 7.10 ppm), H-6 to H-5 (triplet, δ 6.55 ppm), and H-5 to H-4 (doublet, δ 6.45 ppm), the ^1H – ^{13}C -HSQC (Figure 2, spectrum c) correlated the H-4 (δ 6.45/126.7), H-5 (δ 6.55/123.8), H-6 (δ 7.10/130.5), and H-7 (δ 6.81/110.7) to the corresponding ^{13}C chemical shifts. Further strong proof for the preceding assignment order stems from a strong ^1H – ^{13}C -HMBC ($^3J_{\text{CH}}$) correlation of H-4 with spirocenter carbon (C_3/C_2) (Figure 2, spectrum d).

The remaining two quaternary carbons, C_8 (δ 141.4 ppm) and C_9 (δ 123.3 ppm), were identified through ^1H – ^{13}C -HMBC cross peaks ($^3J_{\text{CH}}$) with $\text{C}_4\text{-H}/\text{C}_6\text{-H}$ and $\text{C}_5\text{-H}/\text{C}_7\text{-H}$, respectively. In addition, the NH proton exhibited ^1H – ^{13}C -HMBC ($^3J_{\text{CH}}$) correlation with C_9 and ($^2J_{\text{CH}}$) correlation with C_8 . The chemical shifts of the benzothiazole protons and carbons were identified using $\text{H}_{2''}$ as an access point after identifying $\text{H}_{2''}$ as the doublet at δ 7.74 ppm based on strong ^1H – ^{13}C -HMBC cross peak ($^3J_{\text{CH}}$) with $\text{N-C}_{6''}$ (δ 7.74/151.8), which is anticipated to be the most downfield shift of the benzothiazole benzene ring. Thus, while ^1H – ^1H -COSY correlated $\text{H}_{2''}$ to $\text{H}_{3''}$ (triplet, δ 7.42 ppm), $\text{H}_{3''}$ to $\text{H}_{4''}$ (triplet, δ 7.55 ppm), and $\text{H}_{4''}$ to $\text{H}_{5''}$ (doublet, δ 8.17 ppm), ^1H – ^{13}C -HSQC correlated the $\text{H}_{2''}$ (δ 7.74/121.6), $\text{H}_{3''}$ (δ 7.42/126.1), $\text{H}_{4''}$ (δ 7.55/126.7), and $\text{H}_{5''}$ (δ 8.17/123.8) to the corresponding ^{13}C chemical shifts (Figure 2, spectrum b). Additional verification for the foregoing assignment order stems from strong ^1H – ^{13}C -HMBC ($^3J_{\text{CH}}$) correlations of $\text{H}_{4''}$ with $\text{N-C}_{6''}$ (δ 7.55/151.8) and both $\text{H}_{3''}$ and $\text{H}_{5''}$ with $\text{S-C}_{1''}$ (δ 7.42/8.17/135.5) (Figure 2, spectrum d). The chemical shifts of the 4-nitrophenyl protons and carbons were identified using C_4H as an entry point after identifying $\text{H}_{2''}$ as the doublet at δ 7.82 ppm based on strong ^1H – ^{13}C -HMBC (Figure 2, spectrum d) cross peak ($^3J_{\text{CH}}$) of C_4H with $\text{C}_{2''}$ (δ 5.60/130.9), where the $\text{C}_{2''}$ chemical shift was correlated in the ^1H – ^{13}C -HSQC (Figure 2, spectrum c) to $\text{H}_{2''}$ (δ 7.82) and $\text{H}_{2''}$ was correlated in the ^1H – ^1H -COSY to $\text{H}_{3''}$ (δ 8.21). The ^{13}C chemical shift of the latter was identified through the ^1H – ^{13}C -HSQC spectrum (δ 122.8). The remaining two quaternary carbons, $\text{C}_{1''}$ (δ 143.9 ppm) and $\text{C}_{4''}$ (δ 147.7 ppm), were identified through ^1H – ^{13}C -HMBC cross peaks ($^3J_{\text{CH}}$) with $\text{C}_5\text{-H}_2$ and $\text{C}_{2''}\text{-H}$, respectively. The stereochemistry of the nonequivalent methylene protons of $\text{C}_5\text{, H}_a$ (δ 3.70, dd, $J = 9.6, 8.4$ Hz), and H_b (δ 4.28, app t, $J = 10.2$ Hz) was determined relative to $\text{C}_{4''}\text{-H}$ based on two very strong cross peaks in the ^1H – ^1H -ROESY spectrum between $\text{H}_b/\text{C}_{4''}\text{-H}$ and the 4-nitrophenyl- $\text{H}_{2''}$, indicating the close proximity of the latter to H_b and $\text{C}_{4''}\text{-H}$ more so than H_a . Following the successful assignment of the proton and carbon chemical shifts for the benzothiazole, oxindoline, 4-nitrophenyl, and pyrrolidine rings, the ^1H – ^1H -ROESY spectrum was inspected for crucial proximity correlation contours that could be utilized to assign the relative stereochemistry of the three stereogenic centers. As expected, the *trans* stereochemistry of the benzothiazole and 4-nitrophenyl (stereogenic centers $\text{C}_{4'}$ and C_3') are predictable based on the initial *E*-geometry of the dipolarophile. Indeed the ^1H – ^1H -ROESY spectrum shows no correlation cross peaks between any of the protons of these two rings, precluding the *syn*

stereochemistry. However, two diastereomeric products will form due to the creation of a second spirocenter ($\text{C}_{2'/3}$) during the process. Notably, the ^1H NMR signals of $\text{C}_{4'}\text{-H}$, $\text{C}_5'\text{-H}_a$ and $\text{C}_4\text{-H}$, which incidentally have been previously used in related systems^{13c} to assign the relative stereochemistry of all chiral centers, were most informative and served also herein as key in assigning the relative stereochemistry. Pleasingly, the presence of cross peaks between $\text{C}_{4'}\text{-H}$ and $\text{C}_4\text{-H}$ as well as between $\text{C}_5'\text{-H}_a$ and $\text{C}_4\text{-H}$ indicates proximity and a *syn*-relationship of the $\text{C}_4\text{-H}$ with both, $\text{C}_5'\text{-H}_a$ and $\text{C}_{4'}\text{-H}$.

While the **5g** and **5'g** diastereomers exhibited comparable ^{13}C chemical shifts except for C_2 (δ 160.5 for **5g** vs δ 165.7 for **5'g**) and $\text{C}_{7''}$ (δ 174.5 for **5g** vs δ 176.4 for **5'g**), the magnetic anisotropy resulting from the *syn* stereochemistry of the neighboring benzothiazole and oxindoline aromatic rings due to the inversion of the C_3/C_2' center impacted the chemical shifts of the oxindoline protons to a very significant extent in the **5g** isomer. The $\text{C}_4\text{-H}$, $\text{C}_5\text{-H}$, and $\text{C}_6\text{-H}$ of the **5g** isomer experienced extreme upfield shifting from δ 8.00 ppm to 6.52 ppm, δ 7.26 ppm to 6.57 ppm, and δ 7.40 ppm to 7.09 ppm, respectively. On the contrary, the $\text{C}_7\text{-H}$ experienced downfield shift from δ 6.73 ppm to 6.83 ppm. The significant upfield shift in the resonance of $\text{C}_4\text{-H}$, $\text{C}_5\text{-H}$, and $\text{C}_6\text{-H}$ may be attributed to the shielding cone of the *syn* benzothiazole aromatic system, providing additional evidence to the assigned *syn* stereochemistry.

Reaction Mechanism. As proposed in Scheme 3, the regio- and stereochemistry for the formation of spiro[indoline-3,2'-pyrrolidine]-3'-carbonitriles **5/5'a** rather than the corresponding regioisomers spiro[indoline-3,2'-pyrrolidine]-4'-carbonitriles **6/6'a** are suggested based on electronic and steric factors. The cycloaddition reaction proceeds via “C1-attack” where the nucleophilic carbon of azomethine ylide is with the less hindered/more electrophilic carbon (C1) of the α,β -alkenenitriles **4a–g**. As indicated in Table 1, the *exo*-cycloadduct was consistently obtained as the major diastereomer in all instances.

Computational Approach. Initially, two possible *E* and *Z* configurations of dipolarophiles 2-(benzo[*d*]thiazol-2-yl)-3-(aryl)acrylonitriles **4a–g** were optimized where the *E*-configurations were ~ 6.30 – 4.40 kcal/mol more stable than the *Z*-configurations at B3LYP/cc-pVTZ (Tables S98–S99). Since isomerization of the geometric isomers is not possible under the reaction conditions, calculations and discussion have been limited to the *E*-isomers.

Also, we have investigated the formation of dipole **3** *in situ* by reaction of isatin (**1**) and *N*-methylglycine (**2**). The negative formation energy value confirms the formation of dipole **3**. The optimization of dipole **3** for both the *E*- and *Z*-configuration at B3LYP/cc-pVTZ are shown in Table S1.

Analysis of Frontier Molecular Orbital (FMO) and Conceptual Density Functional Theory (CDFT) Reactivity Indices. Frontier molecular orbital (FMO) which was developed by Fukui¹⁴ is one of the best methods to analyze reactions. 1,3-Dipolar cycloaddition reactions are classified into three types on the basis of the relative FMO energies (HOMO/LUMO interaction) between the dipole and dipolarophile.¹⁵

On the basis of the frontier molecular orbital (FMO) theory, Sustmann classified cycloaddition processes into three distinct types. Type I involves the interaction between the HOMO of the dipole ($\text{HOMO}_{\text{dipole}}$) and the LUMO of the dipolarophile ($\text{LUMO}_{\text{dipolarophile}}$), also known as normal-electron demand (NED) 1,3-dipolar cycloaddition (DC) reactions. This classification encompasses a significant portion of 1,3-DC

Table 2. Frontier Orbital Energies (eV) for Dipole 3 and Dipolarophiles 4a–g at the B3LYP/cc-pVTZ Level of Theory

Reactant	HOMO (eV)	LUMO (eV)	Energy barrier [ΔE , eV] ^{a,b}	
			<i>E</i> -dipole (3)	<i>Z</i> -dipole (3)
<i>E</i> -dipole (3)	 -4.9916	 -1.7095		
<i>Z</i> -dipole (3)	 -5.1016	 -1.8017		
<i>E</i> -4a	 -6.3484	 -2.7851	2.2065 (4.6389)	2.3165 (4.5467)
<i>E</i> -4b	 -6.0222	 -2.5683	2.4233 (4.3127)	2.5333 (4.2205)
<i>E</i> -4c	 -6.2267	 -2.6890	2.3026 (4.5172)	2.4126 (4.4250)
<i>E</i> -4d	 -6.4079	 -2.9292	2.0624 (4.6984)	2.1724 (4.6062)
<i>E</i> -4e	 -6.3733	 -2.8277	2.1639 (4.6638)	2.2739 (4.5716)
<i>E</i> -4f	 -6.6873	 -3.3442	1.6474 (4.9778)	1.7574 (4.8856)
<i>E</i> -4g	 -6.7658	 -3.5525	1.4391 (5.0563)	1.5491 (4.9641)

^a $\Delta E = \text{LUMO}_{(\text{dipolarophile } 4\text{a-g})} - \text{HOMO}_{(\text{dipole } 3)}$ (normal electron demand). ^b $(\Delta E) = \text{LUMO}_{(\text{dipole } 3)} - \text{HOMO}_{(\text{dipolarophile } 4\text{a-g})}$ (inverse electron demand).

reactions. Type II is characterized by the interaction between the LUMO of the dipole and the HOMO of the dipolarophile, termed as inverse-electron demand (IED) 1,3-DC reactions. Lastly, type III involves dipole/dipolarophile pairs with similar HOMO and LUMO energies. In such cases, both LUMO dipolarophile, HOMO dipole and LUMO dipole, HOMO dipolarophile interactions may influence reactivity and

regiochemistry, allowing for the occurrence of both NED and IED processes.

In this study, the HOMO–LUMO energy gaps propose that the $\text{LUMO}_{(\text{dipolarophile})} - \text{HOMO}_{(\text{dipole})}$ interaction controls the cycloaddition reaction (normal electron demand reactions).¹³ The calculated energies of the frontier orbitals for dipole 3 and dipolarophiles 4a–g are presented in Table 2. It is clear that the

energy gaps $\Delta E = \text{LUMO}_{(\text{dipolarophiles } 4\mathbf{a-g})} - \text{HOMO}_{(E\text{-dipole } 3)}$ lower than those of the corresponding *Z*-dipole (**3**) prove the reactions are cycloaddition of *E*-form of dipole (**3**) with the *E*-form of dipolarophiles **4a–g**.

In recent decades, conceptual density functional theory (CDFT) has provided a strong framework for the establishment and development of chemical reactivity theory.^{16,17} The analysis of global and local CDFT reactivity indices in the ground state of reagents in the framework of DFT descriptors is a powerful tool for the description of molecular reactivity in polar processes,^{17,18} especially for a previous study on the polar character of cycloadditions.¹⁹ Likewise, the understanding of electrophilicity/nucleophilicity indices in the context of DFT are powerful tools to explain the behavior of 1,3-dipolar cycloaddition reactions, and it has been successfully used to classify dipole and dipolarophile pairs used in such reactions.²⁰

The ability of a molecule to transfer charge in its ground state, approximated by Koopmans theory, can be described by the electronic chemical potential μ , which is defined as the arithmetic mean of one-electron energies of the frontier molecular orbitals HOMO and LUMO, as $\mu = -(I + A)/2$.²¹ The chemical hardness η , which is a measure of the stability of a system, can be considered as $\eta = (I - A)$ where I (ionization potential) = $-E_{\text{HOMO}}$ and A (electron affinity) = $-E_{\text{LUMO}}$. η can be viewed as a measure of the difficulty of changing the number of electrons in a system, which is conceptually similar to nonpolarizability or hardness. Since softness, S , is the opposite of hardness, it has been defined as the inverse of hardness as $S = 1/\eta$.²² The global electrophilicity index (ω), which measures the stabilization in energy when the system acquires an additional electronic charge from the environment, was given by the following simple expression, $\omega = \mu^2/2\eta$, in terms of the electronic chemical potential μ and the chemical hardness η .²³ The global indices μ , η , S , and ω are calculated and are listed in Table 3.

Table 3. Global Properties and Global Electrophilicity/Nucleophilicity Indices Values for Dipole **3 and Dipolarophiles **4a–g** Involved in the Cycloaddition Reactions^a**

Reactant	μ (eV)	η (eV)	S (a.u.)	ω (eV)	ω^+ (eV)	ω^- (eV)	N° (eV)	N' (eV)	N'' (eV)
(<i>E</i>)-dipole 3	-3.35	3.28	8.30	1.71	0.44	3.80	4.42	0.58	2.63
(<i>Z</i>)-dipole 3	-3.45	3.30	8.25	1.80	0.49	3.94	4.31	0.55	2.54
4a	-4.57	3.56	7.64	2.93	1.09	5.66	3.06	0.34	1.77
4b	-4.29	3.45	7.88	2.67	0.96	5.26	3.39	0.37	1.90
4c	-4.46	3.54	7.69	2.81	1.02	5.48	3.18	0.36	1.82
4d	-4.67	3.48	7.82	3.13	1.23	5.90	3.00	0.32	1.69
4e	-4.60	3.55	7.67	2.98	1.13	5.72	3.04	0.34	1.75
4f	-5.02	3.34	8.15	3.77	1.67	6.69	2.72	0.27	1.49
4g	-5.16	3.21	8.48	4.15	1.97	7.13	2.64	0.24	1.40

^aAll computations were carried out with the Gaussian 09 suite of programs. Calculations based on the method of DFT were performed at the B3LYP/cc-pVTZ level of theory. ^bHOMO energy of tetracyanoethylene (TCE) is -0.34586 (in a.u.) at the same level of theory.

The electronic chemical potential, μ , of dipole **3** is higher than the α,β -alkenenitriles **4a–g** ($-5.16 < \mu < -4.29$ eV); also dipole **3** with configuration "*E*" has an electronic chemical potential ($\mu = -3.35$ eV) higher than its stereoisomer with configuration "*Z*" ($\mu = -3.45$ eV).

Additionally, α,β -alkenenitriles **4a–g** act as electrophiles due to the larger value of their electrophilicity ω ($2.67 < \omega < 4.15$) relative to the electrophilicity value of *E*-dipole **3** ($\omega = 1.71$ eV), and therefore the charge transfer takes place from the *E*-dipole (**3**) to (*E*)-2-(benzo[*d*]thiazol-2-yl)-3-(aryl)acrylonitriles **4a–g** as the dipolarophile.

Recently, Domingo et al. presented a unique electrophilicity scale to classify reagents involved in CA reactions.²⁴ Analysis of the developed electrophilicity indices ω presented in Table 3 indicates that α,β -alkenenitriles **4a–g** are among the strong electrophiles, while dipole **3** is mostly among the marginal electrophiles (nucleophiles), suggesting that in a polar 1,3-dipolar cycloaddition, α,β -alkenenitriles **4a–g** and dipole **3** act as electrophile and nucleophile, respectively. In accordance with this model, the polar character of a dipole-dipolarophile interaction can be evaluated by the difference $\Delta\omega$ in the global electrophilicity of the two reagents.^{24a} It is clear that the 32CA of (**3**) as dipole with (**4a–g**) as dipolarophile ($\Delta\omega$ are in the range of 0.96 and 2.44, $\ll 4.50$ eV) are reactions controlled by a one-step mechanism.

Recently, Gázquez et al.²⁵ proposed new reactivity indices, defined as the electroaccepting, ω^+ [$\omega^+ = A\Delta/2(I - A)$], and electrodonating, ω^- ($\omega^- = I\Delta/2(I - A)$), powers. Where ω^+ represents the measure of the tendency of a given system to accept charge, ω^- is the tendency to release charge. It is noteworthy that a greater ω^+ value of a system reflects a better ability to accept charge, while a smaller value of ω^+ corresponds to a better electron donor. Both quantities are calculated by employing the vertical ionization energy I and electron affinity A and collected in Table 3.

It is important to note that according to these definitions and as mentioned in Table 3, the α,β -alkenenitriles **4f** ($\omega^+ = 1.67$) and **4g** ($\omega^+ = 1.97$) are the molecules with the greater ability to accept charge (strong electrophiles), while the (*E*)-dipole **3** ($\omega^+ = 0.44$) azomethine ylide is the molecule with the greater ability to donate charge (good nucleophile).

On the other hand, the low values of the ω index cannot be directly associated with the nucleophilic character. To obtain a working model descriptor for nucleophilicity, the empirical nucleophilicity index N proposed by the Kohn and Sham based on the HOMO energies can be defined as $N = E_{\text{HOMO}}$ (eV) $- E_{\text{HOMO(TCE)}}$ (eV).²⁶

The nucleophilicity values N for the azomethine ylide dipole **3** and our series of dipolarophiles **4a–g** are presented in Table 3. The nucleophilicity of (*E*)-dipole **3** ($N = 4.42$ eV) shows that it is most nucleophilic toward dipolarophiles **4a–g**.

In addition, we calculated the nucleophilicity based on the assumption of Chattaraj et al. that electrophilicity and nucleophilicity are inversely related.^{27,28} The proposed nucleophilicity parameter was described as the multiplicative inverse of the electrophilicity index (ω) and denoted as $N' = 1/\omega$.^{24,29}

In this sense, Roy et al. proposed the nucleophilicity index, N'' , as the reciprocal of the electrodonating ω^- potency.³⁰ Since the nucleophilicity index determined as $1/\omega^-$ was less than 1, the nucleophilicity index N'' has recently been defined as $N'' = ((1/\omega^-) \times 10)$.^{30,31} As shown in Table 3, the calculated N' and N'' follow the same order as found for the corresponding nucleophilicity N descriptor. Thus, a comparison of the values obtained with the three nucleophilicity models, the nucleophilicity N values with the reciprocal of electrophilicity, N' , and Roy's N'' values, shows reasonable agreement.

Moreover, the regiochemistry of the polar cycloaddition reactions can be investigated using local parameters of reactivity,

Table 4. Nucleophilic and Electrophilic Fukui f_k^\pm , Local Softness s_k^\pm , Parr Indices P_k^\pm , Local Electrophilicity ω_k , and Local Nucleophilicity N_k for the Most Relevant Heavy Atoms of Azomethine Ylide **3 and α,β -Alkenenitriles **4a–g**^a**

Comp.	Site k		f_k^+	f_k^-	s_k^+	s_k^-	P_k^+	P_k^-	ω_k	N_k	R_k
3	3	C	0.27	0.21	2.24	1.74	0.69	0.36	1.18	1.59	± 1.39
	4	C	0.02	0.17	0.16	1.40	-0.04	0.32	-0.07	1.41	± 0.67
4a	1	C	0.15	0.05	1.15	0.38	0.38	0.07	1.11	0.21	+0.90
	2	C	0.08	0.07	0.61	0.53	0.06	0.14	0.18	0.43	-0.25
4b	1	C	0.16	0.01	1.26	0.08	0.40	0.00	1.07	0.00	+1.07
	2	C	0.07	0.10	0.55	0.79	0.05	0.17	0.13	0.58	-0.45
4c	1	C	0.15	0.04	1.15	0.31	0.38	0.04	1.07	0.13	+0.94
	2	C	0.08	0.09	0.62	0.69	0.06	0.16	0.17	0.51	-0.34
4d	1	C	0.14	0.04	1.09	0.31	0.36	0.05	1.13	0.15	+0.98
	2	C	0.08	0.08	0.65	0.60	0.07	0.14	0.22	0.42	-0.20
4e	1	C	0.15	0.04	1.15	0.31	0.39	0.06	1.16	0.18	+0.98
	2	C	0.08	0.08	0.61	0.61	0.06	0.14	0.18	0.43	-0.25
4f	1	C	0.11	0.06	0.90	0.49	0.29	0.08	1.09	0.22	+0.87
	2	C	0.09	0.06	0.73	0.49	0.10	0.11	0.38	0.30	± 0.34
4g	1	C	0.10	0.05	0.83	0.42	0.23	0.10	0.95	0.26	+0.69
	2	C	0.08	0.08	0.67	0.65	0.10	0.10	0.42	0.26	± 0.34

^aCalculations based on the method of DFT were performed at the B3LYP/cc-pVTZ level of theory.

including the condensed Fukui (f_k^\pm), Parr functions analysis (P_k^\pm), local electrophilicity $\omega_k = \omega P_k^+$, and local nucleophilicity $N_k = NP_k^-$ indices.³² The local electrophilic and nucleophilic functions for azomethine ylide dipole **3** and dipolarophiles **4a–g** are summarized in Table 4. Figure 3 shows the atomic spin density (ASD) maps of the radical cation of azomethine ylide **3** and radical anions of alkenes **4a–g** at B3LYP/cc-pVTZ.

The nucleophilic Parr functions, P_k^- , of the azomethine ylide **3** are 0.36 (C3) and 0.32 (C4) and the electrophilic Parr functions P_k^+ of alkene **4a–g** are 0.23–0.40 (C1) and 0.05–0.10 (C2). Consequently, the C3 carbon is the most nucleophilic center of azomethine ylide **3** ($N_k = 1.59$) and C1 is the most electrophilic site of alkene **4** ($\omega_k = 0.95–1.16$). Therefore, the most favorable regioisomeric pathway will be associated with the initial $C_3^{AY}-C_1^{alkene}$ bond formation. These results are consistent with experimental observations demonstrating that the 32CA process between azomethine ylides **3** and alkenes **4a–g** occurs through interaction between $C_3^{AY}-C_1^{alkene}$ and $C_4^{AY}-C_2^{alkene}$, leading to the formation of the pyrrolidine derivatives **5a–g** that facilitate pathway A (C1-attack) (Scheme 2).

To gain a deeper insight into the electrophilic and/or nucleophilic activation at the different sites of a molecule, Chattaraj et al. proposed the local reactivity difference index R_k , which can predict the local electrophilic and/or nucleophilic activation within an organic molecule.³³ The R_k index is defined as

$$\text{if } (1 < \omega_k/N_k < 2 \text{ or } 1 < N_k/\omega_k < 2), \text{ then } R_k \approx (\omega_k + N_k)/2 \Rightarrow \text{ambiphilic } (R_k = \pm x.xx) \quad (\text{a})$$

$$\text{otherwise, } R_k \approx (\omega_k - N_k), \text{ where } R_k > 0 \Rightarrow \text{electrophilic } (R_k = +x.xx) \\ R_k < 0 \Rightarrow \text{nucleophilic } (R_k = -x.xx) \quad (\text{b})$$

From the data (Table 4) for dipolarophiles **4a–g**, the C1 site is more electrophilic than C2 (C1, $R_k = +0.69 - +1.07$; C2, $R_k = -0.45 - \pm 0.34$).

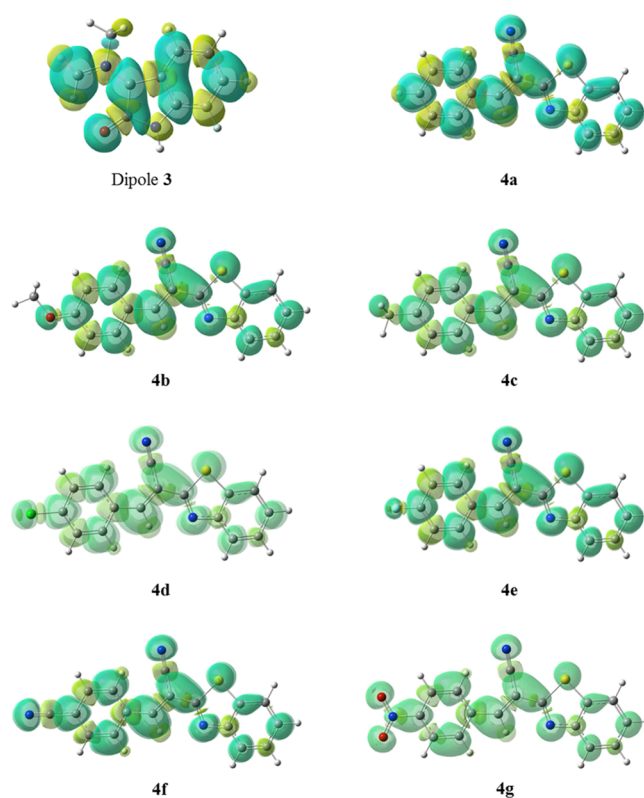
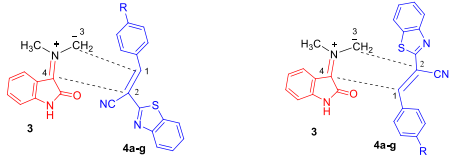


Figure 3. Atomic spin density (ASD) maps of the radical cation of azomethine ylide **3** and radical anions of alkenes **4a–g** at B3LYP/cc-pVTZ.

On the other hand, the hard and soft acids and bases (HSAB) principle³⁴ and the local softness s_k^\pm can be used to predict the regioselectivity of 32CA reactions.³⁵ Accordingly, the interacting atoms for the preferred regioisomeric pathway of a 32CA reaction have approximately equal softness values. The local softness values s_k^\pm are calculated by $s_k^\pm = S f_k^\pm$,³⁶ where S is the global softness and f_k^\pm are the respective Fukui functions. The

softness matching index ΔS_{ab}^{cd} calculated by $\Delta S_{ab}^{cd} = (s_a^- - s_c^+)^2 + (s_b^- - s_d^+)^2$. s_a^- and s_b^- are the softness values for the electrophilic attack for the two atoms of the dipole involved in the cycloaddition, while s_c^+ and s_d^+ are the softness for the nucleophilic attack for the two atoms of the dipolarophile involved in the 32CA reaction, with the lower value of ΔS_{ab}^{cd} indicating the preferred pathway. For 32CA of azomethine ylide **3** and alkene **4**, the ΔS_{34}^{12} value for the formation of regioisomer **5** ($\Delta S_{34}^{12} = 0.95$ – 1.36) is smaller than that for **6** ($\Delta S_{34}^{21} = 1.27$ – 1.47), supporting pathway A (Table 5).

Table 5. Softness Matching Index ΔS_{ab}^{cd} of Possible Pathways for the Cycloaddition Reaction of Azomethine Ylide **3 and α,β -Alkenenitriles **4a–g****



Reactants	Pathway A (C1-attack)	Pathway B (C2-attack)
	$\Delta S_{34}^{12} = (s_{k3}^- - s_{k1}^+)^2 + (s_{k4}^- - s_{k2}^+)^2$	$\Delta S_{34}^{21} = (s_{k3}^- - s_{k2}^+)^2 + (s_{k4}^- - s_{k1}^+)^2$
3 + 4a	0.97	1.34
3 + 4b	0.95	1.43
3 + 4c	0.96	1.32
3 + 4d	0.99	1.28
3 + 4e	0.97	1.34
3 + 4f	1.15	1.27
3 + 4g	1.36	1.47

Interestingly, a plot of electrophilicity difference ($\Delta\omega = \omega_{(alkene)} - \omega_{(E-dipole)}$) against softness matching index (ΔS_{34}^{12}) shows a linear graph with a strong correlation ($R^2 = 0.93$) as shown in Figure 4, while no correlation occurs against a ΔS_{34}^{21} facilitating pathway A (C1 attack).

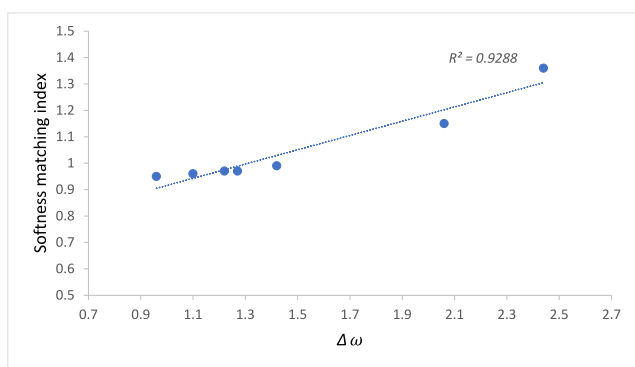


Figure 4. A plot of electrophilicity difference ($\Delta\omega$) against softness matching index (ΔS_{34}^{12}) of CA addition reactions of azomethine ylide **3** and alkenes **4a–g**.

Electrostatic Potential Distribution (ESP). The molecular surface is a useful simulation technique for the model of quantitative molecular surface analysis, which allows us to distinguish the location of the electron density.³⁷ The electrostatic potential map helps to analyze the distribution of charges in several types of molecules, including organic substances. Lately, the molecular electrostatic potential (MESP) has been used to predict the probable site of molecules

for cycloaddition reactions. While it has been used extensively to interpret and predict the reaction behavior of molecules, electrostatic effects can also contribute to regioselectivities.³⁸

To explore the local reactivity indices mentioned earlier, the electrostatic potential distribution (ESP) pattern of the starting materials azomethine ylide **3** and α,β -alkenenitriles **4a–g** has been generated and is presented in Figure 5. The surface area of the individual molecules has been established as the isosurface of density $\rho = 0.001$, and the color values are given in kcal/mol. The red color represents the zone with the negative potential of MEP, associated with reactive electrophilic sites, and the blue color is adapted to the zone with the positive potential and represents the suitable center of the nucleophilic attacks.

From Figure 5, it is evident that the C1 center in alkenes **4a–g** are located in the zone with the positive potential, confirming their high electrophilicity indices to be the more proper center of nucleophilic attack compared to the C2 center, supporting formation of regioisomeric adduct **5** as a major product (pathway A).

These results were found to be in exact agreement with the experimental observations, thus confirming the accuracy of the calculated descriptors for the local electrophilicity and nucleophilicity of the reactants. These descriptors successfully explained the regioselective behavior of the dipoles and dipolarophiles in the 32CA reaction and provided insights into the underlying mechanism of regioselectivity.

Energies of Transition-State Structures. Although the FMO theory, based on electronic factors without consideration of steric factors, provides a good basis for understanding the regioselectivity of 32CA reactions, in many cases steric factors control the regiochemistry of the reaction.³⁹

Experimentally, it was observed that the cycloaddition reactions of isatin (**1**), *N*-methylglycine (**2**), and dipolarophiles **4a–g** are regiospecific. Only a single regioisomer of **5a–g** was obtained through pathway A (C1-attack), while the formation of the other regioisomer **6a–g** was not observed at all.

Hypothetically, the reaction could proceed via pathway A (C1-attack) or pathway B (C2-attack), and in both cases the orientation of the reactants could be *endo* or *exo*. Therefore, a computational study was carried out to determine the energetics of reaction pathways A and B through the *exo* and *endo* transition states for the formation of possible regioisomers **5a/5'a** and **6a/6'a**, respectively, starting from azomethine ylide **3** and alkenes **4a** (Figure 6). The stereoselectivity of the reaction of azomethine ylide **3** and alkene **4a** can be rationalized by considering the activation and reaction energies, enthalpies, and Gibbs free energies of the possible pathways A and B for the formation of the possible stereoisomeric products **5/5'** and **6/6'** via the *exo*- and *endo*-TS, respectively (Table 6). In the gas phase, the calculated relative Gibbs free energies of activation associated with possible pathways of this 32CA reaction at B3LYP/cc-pVTZ are 22.27 (**5(TS-I)**), 26.77 (**5(TS-II)**), 33.16 (**6(TS-I)**), and 33.33 kcal/mol (**6(TS-II)**). The TSs associated with regioisomeric pathway **5** show lower activation energies than pathway **6**. This finding indicates that regioisomeric pathway **5** is the exclusive product of the cycloaddition reaction, demonstrating high regioselectivity in all cases. However, for both the regioisomeric pathway, the *exo* approaches have smaller activation free energies than *endo* approaches. In the gas phase, the free energy of **5(TS-I)** is 4.50 kcal/mol lower than that of **5(TS-II)**, favoring the formation of the stereoisomer **5a** as a major product which is in agreement with experimental outcomes (Scheme 3). The geometries of the products and

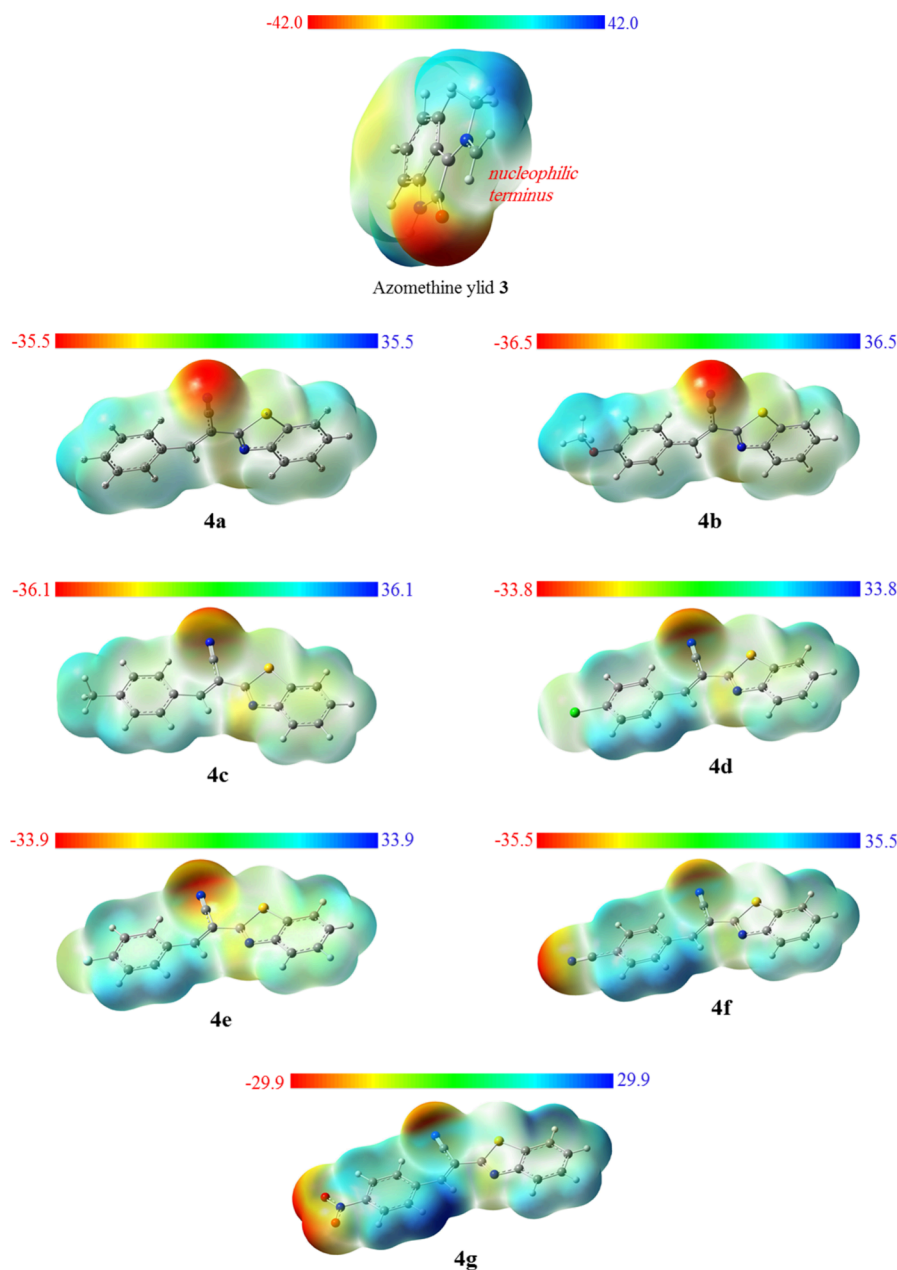


Figure 5. Electrostatic potential (ESP) maps of azomethine ylide **3** and alkenes **4a–g** (B3LYP/cc-pVTZ, kcal/mol).

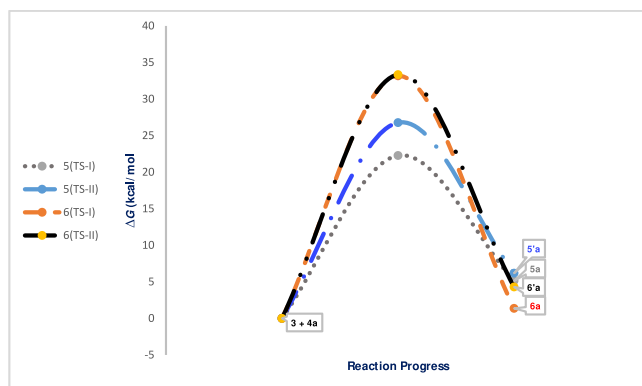


Figure 6. Relative energies (kcal/mol) for the reactants (**3** + **4a**), TSs, and products for the four possible reaction pathways.

TSs for the possible reaction pathways of azomethine ylide **3** and alkene **4a** are given in Figure 7.

Table 6 also shows bond length differences (ΔR) of the two forming bonds of the possible TSs. Accordingly, regioisomeric pathway **5** is more asynchronous than the other pathway (pathway **6**).

On the other hand, the polarity of the reaction seems to be an important factor that determines the feasibility of the reaction. The global electron density transfer (GEDT) was computed by the sum of the natural atomic charges (q), which were obtained by a natural population analysis (NPA), and in which the atoms belonged to each framework (f) at the TSs,⁴⁰ $\text{GEDT}(f) = \sum_{q \in f} q$, which fluxes from dipole **3** toward the alkene **4** framework. Along the possible reaction pathways, the GEDT values at the TSs given in Figure 7 are 0.32e at **5(TS-I)**, 0.28e at **5(TS-II)**, 0.25e at **6(TS-I)**, and 0.23e at **6(TS-II)**. These values highlight the highly polar nature of the reaction. A good correlation

Table 6. Calculated Electronic Activation Energies E_a , Reaction Enthalpies ΔH , Reaction Gibbs Free Energies ΔG , Reaction Energies ΔE_{rxn} , Activation Enthalpies ΔH^\ddagger , Activation Gibbs Free Energies ΔG^\ddagger (in kcal/mol) and Reaction Entropies ΔS (in cal/mol K), and Bond Length Differences ΔR (in Å) for the Cycloaddition Reaction of Azomethine Ylide 3 and Alkene 4a at the B3LYP/cc-pVTZ Level

Structure	E_a	ΔH	ΔG	ΔE_{rxn}	ΔH^\ddagger	ΔG^\ddagger	ΔS	ΔR
5(TS-I)	7.36	-9.93	5.14	-12.05	8.03	22.27	-50.52	0.93
5(TS-II)	11.99	-9.53	6.18	-11.75	12.74	26.77	-52.70	0.92
6(TS-I)	18.65	-13.29	1.37	-15.61	19.12	33.16	-49.19	0.37
6(TS-II)	18.45	-10.78	4.29	-13.17	18.98	33.33	-50.57	0.60

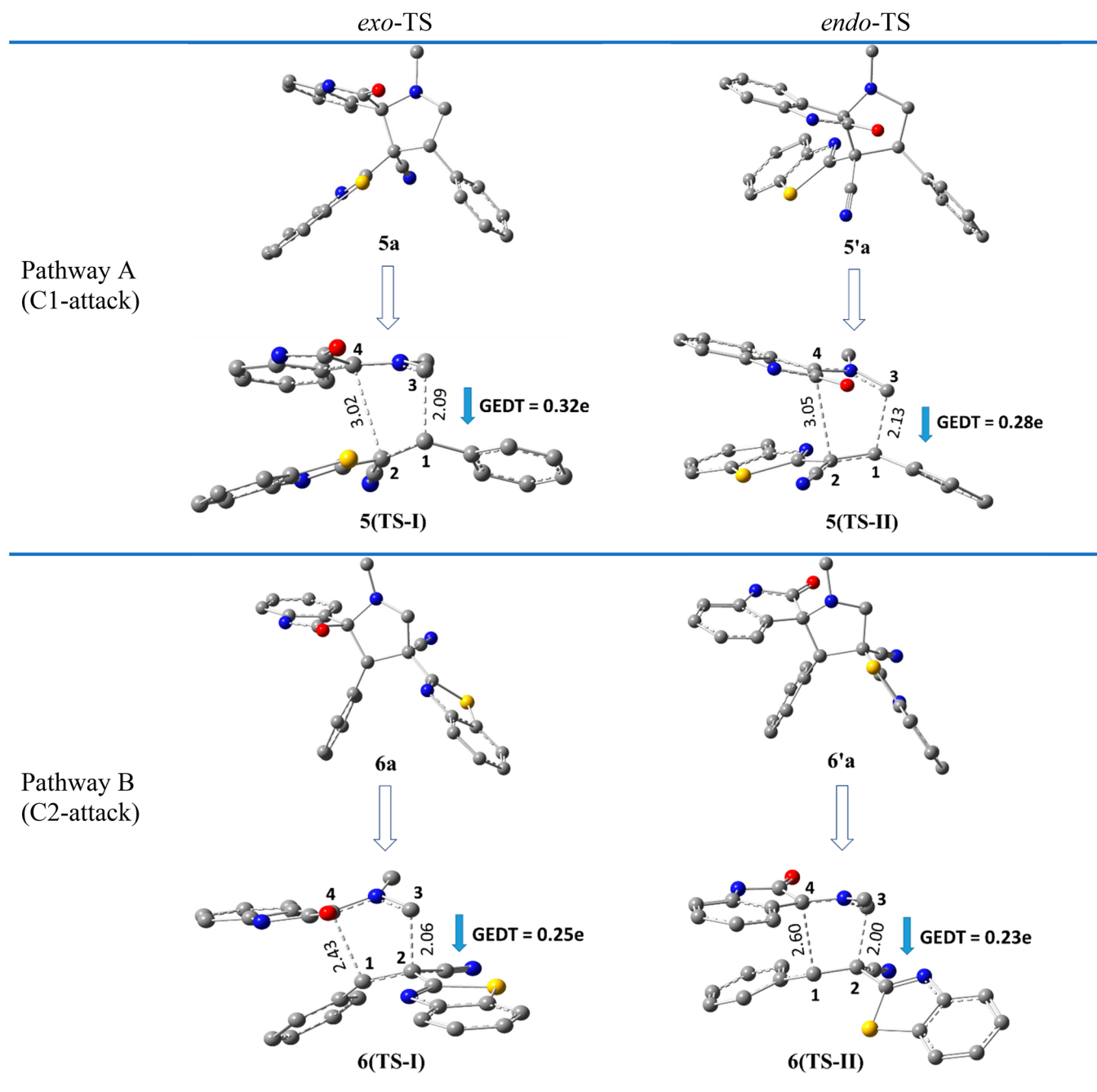


Figure 7. Optimized products and transition state geometries and global electron density transfer (GEDT) at *exo*-TS and *endo*-TS in the cycloaddition reaction of dipole 3 with alkene 4a in possible pathways A and B at the B3LYP/cc-pVTZ level. The C3...C1/C4...C2 (pathway A) and C3...C2/C4...C1 (pathway B) bond distance (\AA) are shown in dashed lines. The blue arrow indicates the direction of GEDT.

between GEDT values at TS and the computed relative free energy of activation (ΔG^\ddagger) can be established ($R^2 = 0.95$).

Hence, this is consistent with the fact that the higher GEDT, the easier bonding changes, lower free energy of activation, and the

faster the reaction,⁴⁰ which is in agreement with the experimental outcomes (Figure 8).

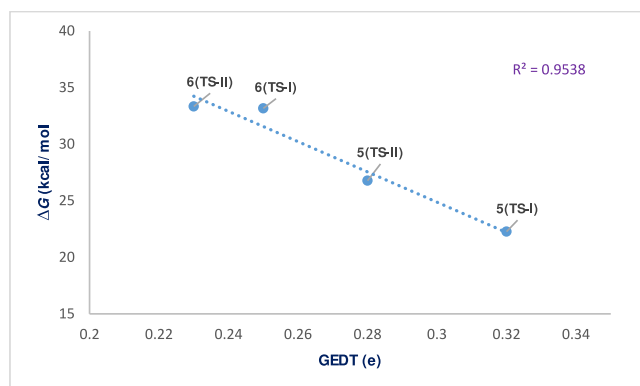


Figure 8. Plot of the activation free energies vs GEDT at TSs for the cycloaddition reaction of dipole **3** with alkene **4a** in possible pathways A and B at the B3LYP/cc-pVTZ level.

Furthermore, the observed stereochemistry can be explained by analyzing the molecular electrostatic potential (MESP) map and studying the electrostatic interactions. Figure 9 shows that in the energetically more favorable transition state **5(TS-I)**, approach of the reactants superimposes the oppositely charged regions, which leads to attractive forces between two fragments. On the other hand, in the energetically less favorable transition states **5(TS-II)**, **6(TS-I)**, and **6(TS-II)**, regions with the same charge are forced to lie over each other, which leads to repulsive forces between two fragments. Therefore, due to the electrostatic attractive forces between two interacting fragments, the

formation of **5(TS-I)** is more favorable than the formation of **5(TS-II)**, **6(TS-I)**, or **6(TS-II)**, which is fully consistent with the experimental results.

CONCLUSION

In summary, we have developed an efficient method for the synthesis of novel spirooxindole-pyrrolidine-benzothiazoles via a one-pot three-component regio- and stereoselective 1,3-dipolar cycloaddition reaction. This reaction involves the *in situ* generation of nonstabilized azomethine ylides by decarboxylative condensation of isatin and *N*-methylglycine, followed by their reaction with various (*E*)-2-(benzo[*d*]thiazol-2-yl)-3-(aryl)acrylonitriles. The obtained products were characterized using 1D and 2D-NMR spectroscopy, confirming their regio- and stereochemistry. The regioselective cycloaddition reactions proceed via pathway A (C1-attack), resulting in a single regioisomer. The pure *exo*- and *endo*-products were isolated using chromatographic techniques. The computational analysis revealed that the *exo*-transition state displays the lowest activation energy among the potential pathways, which is in accordance with the experimental observations.

The investigation of the electrophilic/nucleophilic properties of azomethine ylide **3** and the α,β -alkenenitriles **4a–g** involved in the polar cycloaddition reactions was conducted. The mechanism, direction of charge transfer, and regioselectivity of these cycloaddition reactions were investigated using global and local electrophilicity and nucleophilicity indices as well as HSAB principle and agreed closely with the experimental results.

Specifically, the analysis of local reactivity indices indicated that the C3 carbon is the most nucleophilic center of azomethine ylide **3**, while the C1 site of alkene **4** is the most electrophilic. These findings were consistent with the experimental observa-

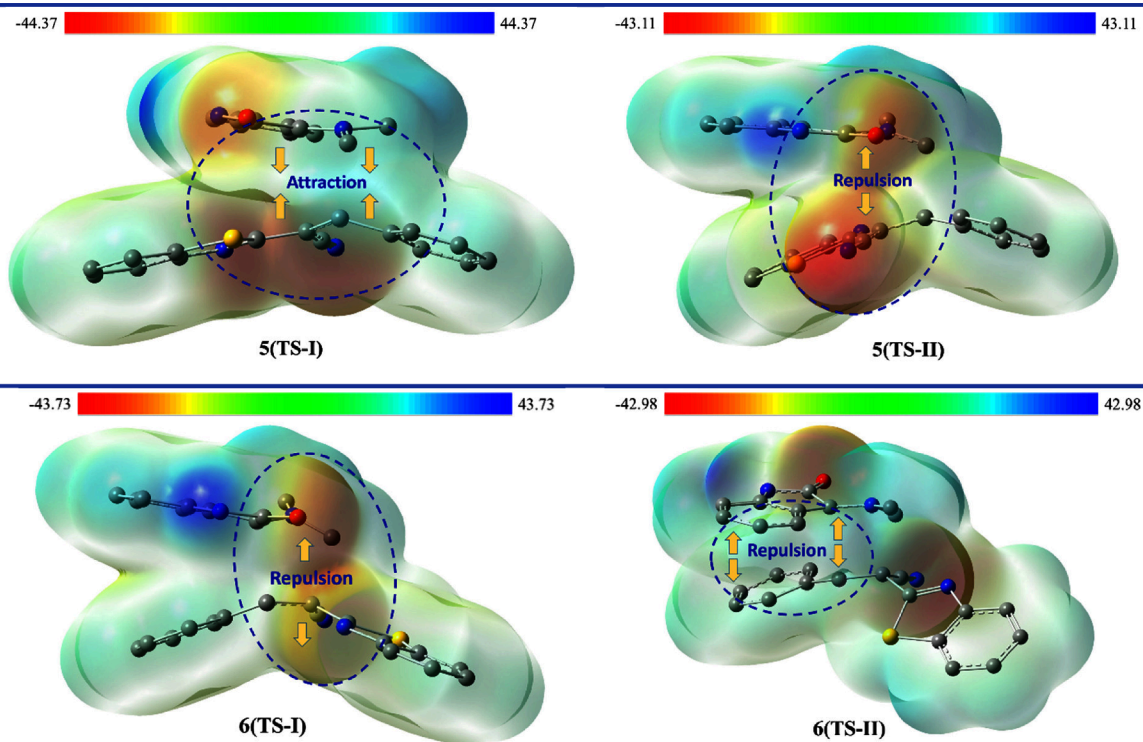


Figure 9. Molecular electrostatic potential MESP maps of the transition states associated with the possible regioisomeric attacks. The blue and red colors display low and high electron density regions, respectively ($\rho = 0.001$ at B3LYP/cc-pVTZ, kcal/mol).

tions, which demonstrated that the 1,3-dipolar cycloaddition process between azomethine ylide **3** and alkenes **4a–g** occurs through interaction between $C_3^{AY}-C_1^{alkene}$ and $C_4^{AY}-C_2^{alkene}$, resulting in the formation of the pyrrolidine derivatives **5a–g**.

The global electron density transfer (GEDT) analysis indicates that the reactions are polar and electron density fluxes from azomethine ylide **3** toward alkenes **4a–g**. The MESP map showed that at the more favorable transition state **5(TS-I)**, approach of reactants locates the oppositely charged regions over each other, resulting in attractive forces between both reactants.

EXPERIMENTAL SECTION

All solvents purchased from Sigma-Aldrich are spectroscopic grade and used without further purification. Melting points were determined on a Stuart SMP3 melting point apparatus and are uncorrected. NMR spectra were recorded on a Bruker Avance III HD NMR spectrometer (600 MHz for 1H , 150 MHz for ^{13}C) in $CDCl_3$ solutions, with residual solvent signals as internal standard. Elemental analyses were performed on a Vario EL v2.3 elemental analyzer; the results were found to be in good agreement with the calculated values ($\pm 0.3\%$). Structural assignments were made with additional information from gCOSY, gHSQC, and gHMBC experiments. The dipolarophiles (*E*)-2-(benzo[*d*]thiazol-2-yl)-3-(aryl)acrylonitriles **4a–g** were prepared according to literature.⁴¹

Computational Details. Geometry optimizations were computed on **1**, **2**, **3**, **4a–g**, **5a–g**, and **6a–g** in vacuum with density functional theory (DFT) using B3LYP exchange correlation functional⁴² combined with Dunning's correlation consistent triple- ζ basis set (cc-pVTZ). Regional Fukui functions for electrophilic (f_k^-) and nucleophilic (f_k^+) attacks were calculated employing the natural population analysis (NPA) at the B3LYP/cc-pVTZ level of theory.⁴³

The electrophilic, (P_k^+), and nucleophilic, (P_k^-), Parr functions were obtained through the analysis of the Mulliken ASD of the radical anion and the radical cation by single-point energy calculations over the optimized neutral geometries using the unrestricted UB3LYP/cc-pVTZ formalism for radical species (Figure 2).^{33d}

Synthetic Procedure. General Procedure for the Synthesis of 3'-(Benzo[*d*]thiazol-2-yl)-1'-methyl-2-oxo-4'-(aryl)spiro[indoline-3,2'-pyrrolidine]-3'-carbonitriles. A mixture of isatin **1** (220 mg, 1.50 mmol), sarcosine **2** (133 mg, 1.50 mmol), and alkene **4** (1.25 mmol) in absolute ethanol (15 mL) was stirred at reflux in an oil bath for 2–5 h. After completion of the reaction (TLC), it was cooled to room temperature and the solvent was removed *in vacuo*. The crude product was chromatographed on silica gel (high-purity grade, pore size 60 Å, 230–400 mesh particle size, 40–63 μm particle size) using dichloromethane as eluent to obtain the pure cycloadducts **5a–g**, **5'c**, **5'f**, and **5'g**.

(2'*S*,3'*R*,4'*R*)-3'-(Benzo[*d*]thiazol-2-yl)-1'-methyl-2-oxo-4'-phenylspiro[indoline-3,2'-pyrrolidine]-3'-carbonitrile (**5a**). Yield: 302 mg (55.4%) from 327 mg of **4a**; white crystals, mp 127–129 °C. 1H NMR ($CDCl_3$, 600 MHz): δ 8.01 (d, *J* = 7.8 Hz, 1H, C_4-H), 7.99 (d, *J* = 7.8 Hz, 1H, C_5-H), 7.71 (s, 1H, N_1-H), 7.69 (d, *J* = 7.2 Hz, 2H, 2 $C-H_{ph}$), 7.65 (d, *J* = 7.8 Hz, 1H, C_2-H), 7.40 (t, *J* = 7.8 Hz, 1H, C_4-H), 7.36–7.30 (m, 4H, 3 $C-H_{ph}$, C_6-H), 7.26 (t, *J* = 7.8 Hz, 1H, C_5-H), 7.23 (t, *J* = 7.8 Hz, 1H, C_3-H), 6.71 (d, *J* = 7.8 Hz, 1H, C_7-H), 5.71 (dd, *J* = 10.2, 7.2 Hz, 1H, C_4-H), 3.87 (app t, *J* = 10.2 Hz, 1H, C_5-H_a), 3.83 (dd, *J* = 9.6, 7.2 Hz, 1H, C_5-H_b), 2.22 (s, 3H, N_1-CH_3) ppm;

^{13}C NMR (150 MHz, $CDCl_3$): δ 175.3 (q, $C_2=O$), 161.3 (q, C_7-H), 152.1 (q, C_6-H), 141.9 (q, C_8), 136.7 (q, C_1-H), 135.5 (q, C_1-H), 130.8 (C_6H), 129.9 (2 C_2-H_{ph}), 128.3 (2 C_3-H_{ph}), 128.0 (C_4-H_{ph}), 126.9 (C_4-H), 126.2 (C_4-H), 125.8 (C_3-H), 124.0 (C_5-H), 123.5 (q, C_9), 123.3 (C_5-H), 121.4 (C_2-H), 117.9 (CN), 109.8 (C_7H), 76.8 (C_3/C_2), 62.0 (C_3), 56.9 (C_5-H_2), 47.3 (C_4-H), 35.5 (N_1-CH_3) ppm. Anal. Calcd for $C_{26}H_{20}N_4OS$: C, 71.54; H, 4.62; N, 12.83. Found: C, 71.31; H, 4.97; N, 12.97.

(2'*S*,3'*R*,4'*R*)-3'-(Benzo[*d*]thiazol-2-yl)-4'-(4-methoxyphenyl)-1'-methyl-2-oxospiro[indoline-3,2'-pyrrolidine]-3'-carbonitrile (**5b**). Yield: 485 mg (83.2%) from 365 mg of **4b**; paige crystals, mp 137–139 °C. 1H NMR ($CDCl_3$, 600 MHz): δ 8.01 (d, *J* = 7.8 Hz, 1H, C_4-H), 8.00 (d, *J* = 7.8 Hz, 1H, C_5-H), 8.01 (d, *J* = 9.0 Hz, 2H, Ar- $C_2-H_{p-methoxyphenyl}$), 7.67 (d, *J* = 7.8 Hz, 1H, C_2-H), 7.61 (d, *J* = 9.0 Hz, 2H, Ar- $C_3-H_{p-methoxyphenyl}$), 7.50 (s, 1H, N_1-H), 7.41 (t, *J* = 7.8 Hz, 1H, C_4-H), 7.34 (t, *J* = 7.8 Hz, 1H, C_6-H), 7.33 (d, *J* = 7.8 Hz, 1H, C_3-H), 7.22 (t, *J* = 7.8 Hz, 1H, C_5-H), 6.73 (d, *J* = 7.8 Hz, 1H, C_7-H), 5.65 (dd, *J* = 10.2, 7.2 Hz, 1H, C_4-H), 3.85 (app t, *J* = 10.2 Hz, 1H, C_5-H_a), 3.82 (dd, *J* = 9.6, 7.2 Hz, 1H, C_5-H_b), 3.76 (s, 3H, OCH_3), 2.24 (s, 3H, N_1-CH_3) ppm; ^{13}C NMR (150 MHz, $CDCl_3$): δ 175.2 (q, $C_2=O$), 161.4 (q, C_7-H), 159.3 (C_4-H), 152.2 (q, C_6-H), 141.9 (q, C_8), 135.5 (q, C_1-H), 131.0 (2 $CH_{p-methoxyphenyl}$), 130.7 (C_6H), 128.4 (q, C_1-H), 126.9 (C_4-H), 126.2 (C_4-H), 125.8 (C_3-H), 124.0 (C_5-H), 123.6 (q, C_9), 123.3 (C_5-H), 121.4 (C_2-H), 118.0 (CN), 113.7 (2 $CH_{p-methoxyphenyl}$), 109.7 (C_7H), 78.7 (C_3/C_2), 62.2 (C_3), 57.2 (C_5-H_2), 55.2 (OCH_3), 46.8 (C_4-H), 35.5 (N_1-CH_3) ppm. Anal. Calcd for $C_{27}H_{22}N_4O_2S$: C, 69.51; H, 4.75; N, 12.01. Found: C, 69.32; H, 4.89; N, 12.04.

(2'*S*,3'*R*,4'*R*)-3'-(Benzo[*d*]thiazol-2-yl)-1'-methyl-2-oxo-4'-*p*-tolylspiro[indoline-3,2'-pyrrolidine]-3'-carbonitrile (**5c**). Yield: 298 mg (53%) from 345 mg of **4c**; pale yellow crystals, mp 132–133 °C. 1H NMR ($CDCl_3$, 600 MHz): δ 8.37 (s, 1H, N_1-H), 7.99 (d, *J* = 7.2 Hz, 1H, C_4-H), 7.89 (d, *J* = 8.4 Hz, 1H, C_5-H), 7.58 (d, *J* = 7.8 Hz, 1H, C_2-H), 7.56 (d, *J* = 7.8 Hz, 2H, Ar- $C_2-H_{p-tolyl}$), 7.32 (t, *J* = 7.8 Hz, 2H, C_6-H , C_4-H), 7.26 (t, *J* = 7.8 Hz, 1H, C_3-H), 7.20 (t, *J* = 7.8 Hz, 1H, C_5-H), 7.12 (d, *J* = 9.0 Hz, 2H, Ar- $C_3-H_{p-tolyl}$), 6.73 (d, *J* = 7.8 Hz, 1H, C_7-H), 5.65 (dd, *J* = 9.6, 7.2 Hz, 1H, C_4-H), 3.84–3.75 (m, 2H, C_5-H), 2.27 (s, 3H, Ar- CH_3), 2.14 (s, 3H, N_1-CH_3) ppm; ^{13}C NMR (150 MHz, $CDCl_3$): δ 175.8 (q, $C_2=O$), 161.3 (q, C_7-H), 152.0 (q, C_6-H), 142.1 (q, C_8), 137.6 (Ar- C_4), 135.3 (q, C_1-H), 133.4 (q, C_1-H), 130.7 (C_6H), 129.7 (2 $C_2-H_{p-tolyl}$), 129.0 (2 $C_3-H_{p-tolyl}$), 126.7 (C_4-H), 126.1 (C_4-H), 125.7 (C_3-H), 123.8 (C_5-H), 123.5 (q, C_9), 123.2 (C_5-H), 121.3 (C_2-H), 117.9 (CN), 110.0 (C_7-H), 78.8 (C_3/C_2), 62.0 (C_3), 56.9 (C_5-H_2), 47.1 (C_4-H), 35.3 (N_1-CH_3), 21.0 (Ar- CH_3) ppm. Anal. Calcd for $C_{27}H_{22}N_4OS$: C, 71.98; H, 4.92; N, 12.44. Found: C, 71.69; H, 5.07; N, 12.67.

(2'*R*,3'*R*,4'*R*)-3'-(Benzo[*d*]thiazol-2-yl)-1'-methyl-2-oxo-4'-*p*-tolylspiro[indoline-3,2'-pyrrolidine]-3'-carbonitrile (**5'c**). Yield: 224 mg (39.8%) from 345 mg of **4c**; yellow crystals, mp 125–126 °C. 1H NMR ($CDCl_3$, 600 MHz): δ 9.21 (s, 1H, N_1-H), 8.09 (d, *J* = 8.4 Hz, 1H, C_5-H), 7.67 (d, *J* = 8.4 Hz, 1H, C_2-H), 7.53 (d, *J* = 7.8 Hz, 2H, Ar- $C_2-H_{p-tolyl}$), 7.46 (t, *J* = 7.2 Hz, 1H, C_4-H), 7.35 (t, *J* = 7.2 Hz, 1H, C_3-H), 7.14 (d, *J* = 7.8 Hz, 2H, Ar- $C_3-H_{p-tolyl}$), 7.03 (t, *J* = 7.8 Hz, 1H, C_6-H), 6.81 (d, *J* = 7.8 Hz, 1H, C_7-H), 6.65 (d, *J* = 7.8 Hz, 1H, C_4-H), 6.58 (t, *J* = 7.8 Hz, 1H, C_5-H), 5.42 (app t, *J* = 9.0 Hz, C_4-H), 4.23 (app t, *J* = 9.6 Hz, 1H, C_5-H_b), 3.60 (app t, *J* = 9.0 Hz, 1H, C_5-H_a), 2.29 (s, 3H, Ar- CH_3), 2.27 (s, 3H, N_1-CH_3) ppm; ^{13}C NMR

(150 MHz, CDCl₃): δ 176.6 (q, C₂=O), 166.1 (q, C_{7'''}), 152.0 (q, C_{6'''}), 141.4 (q, C₈), 137.9 (Ar-C_{4'}), 135.4 (q, C_{1'''}), 133.0 (q, C_{1''}), 130.1 (C₆H), 129.6 (2C_{2''}-H_{p-tolyl}), 129.2 (2C_{3''}-H_{p-tolyl}), 126.3 (C₄-H), 126.1 (C_{4'''}-H), 125.8 (C_{3'''}-H), 123.7 (q, C₉), 123.6 (C_{5'''}-H), 122.3 (C₅-H), 121.4 (C_{2'''}-H), 118.2 (CN), 110.6 (C₇H), 80.1 (C₃/C_{2'}), 61.3 (C_{3'}), 57.5 (C₅-H₂), 51.5 (C₄-H), 35.5 (N₁-CH₃), 21.1 (ArCH₃) ppm. Anal. Calcd for C₂₇H₂₂N₄OS: C, 71.98; H, 4.92; N, 12.44. Found: C, 71.60; H, 5.11; N, 12.71.

(2',3',3',4',4',3')-(Benzo[d]thiazol-2-yl)-4'-(4-chlorophenyl)-1'-methyl-2-oxospiro[indoline-3,2'-pyrrolidine]-3'-carbonitrile (**5d**). Yield: 310 mg (52.7%) from 371 mg of **4d**; pale yellow crystals, mp 141–143 °C. ¹H NMR (CDCl₃, 600 MHz): δ 7.99 (d, J = 7.2 Hz, 1H, C₄-H), 7.97 (d, J = 8.4 Hz, 1H, C_{5'''}-H), 7.87 (s, 1H, N₁-H), 7.65 (d, J = 8.4 Hz, 1H, C_{2'''}-H), 7.63 (d, J = 8.4 Hz, 2H, Ar-C_{2''}-H_{p-chlorophenyl}), 7.40 (t, J = 7.8 Hz, 1H, C_{4'''}-H), 7.36 (t, J = 7.8 Hz, 1H, C₆-H), 7.32 (t, J = 7.8 Hz, 1H, C_{3'''}-H), 7.29 (d, J = 8.4 Hz, 2H, Ar-C_{3''}-H_{p-chlorophenyl}), 7.23 (t, J = 7.2 Hz, 1H, C₅-H), 6.72 (d, J = 7.8 Hz, 1H, C₇-H), 5.72 (dd, J = 10.8, 7.2 Hz, 1H, C₄-H), 3.85 (app t, J = 10.2 Hz, 1H, C₅-H_a), 3.78 (dd, J = 9.6, 7.2 Hz, 1H, C₅-H_b), 2.19 (s, 3H, N₁-CH₃) ppm; ¹³C NMR (150 MHz, CDCl₃): δ 175.2 (q, C₂=O), 161.0 (q, C_{7'''}), 152.0 (q, C_{6'''}), 142.0 (q, C₈), 135.5 (q, C_{1''}), 135.2 (q, C_{1'''}), 133.9 (ArC_{4'}-Cl), 131.3 (2C_{2''}-H_{p-chlorophenyl}), 130.9 (C₆H), 128.5 (2C_{3''}-H_{p-chlorophenyl}), 126.8 (C₄-H), 126.3 (C_{4'''}-H), 125.9 (C_{3'''}-H), 124.0 (C_{5'''}-H), 123.3 (C₅-H), 123.2 (q, C₉), 121.4 (C_{2'''}-H), 117.7 (CN), 109.9 (C₇H), 78.7 (C₃/C_{2'}), 61.9 (C₃), 56.7 (C₅-H₂), 46.5 (C₄-H), 35.4 (N₁-CH₃) ppm. Anal. Calcd for C₂₆H₁₉ClN₄OS: C, 66.31; H, 4.07; N, 11.90. Found: C, 66.59; H, 3.88; N, 11.77.

(2',3',3',4',4',3')-(Benzo[d]thiazol-2-yl)-4'-(4-fluorophenyl)-1'-methyl-2-oxospiro[indoline-3,2'-pyrrolidine]-3'-carbonitrile (**5e**). Yield: 548 mg (96.5%) from 350 mg of **4e**; pale yellow crystals, mp 183–185 °C. ¹H NMR (CDCl₃, 600 MHz): δ 8.09 (s, 1H, N₁-H), 7.99 (d, J = 7.2 Hz, 1H, C₄-H), 7.95 (d, J = 8.4 Hz, 1H, C_{5'''}-H), 7.66 (dd, J = 8.4, 5.4 Hz, 2H, Ar-C_{2''}-H_{p-fluorophenyl}), 7.63 (d, J = 7.8 Hz, 1H, C_{2'''}-H), 7.37 (t, J = 8.4 Hz, 1H, C_{4'''}-H), 7.35 (t, J = 8.4 Hz, 1H, C₆-H), 7.30 (t, J = 7.2 Hz, 1H, C_{3'''}-H), 7.22 (t, J = 7.8 Hz, 1H, C₅-H), 7.00 (d, J = 8.4 Hz, 2H, Ar-C_{3''}-H_{p-fluorophenyl}), 6.74 (d, J = 7.8 Hz, 1H, C₇-H), 5.72 (dd, J = 10.2, 6.6 Hz, 1H, C₄-H), 3.84 (app t, J = 10.2 Hz, 1H, C₅-H_a), 3.78 (dd, J = 9.6, 7.2 Hz, 1H, C₅-H_b), 2.17 (s, 3H, N₁-CH₃) ppm; ¹³C NMR (150 MHz, CDCl₃): δ 175.4 (q, C₂=O), 162.4 (d, J = 244.5 Hz, ArC_{4'}-F), 161.0 (q, C_{7'''}), 152.0 (q, C_{6'''}), 142.0 (q, C₈), 135.4 (q, C_{1'''}), 132.3 (d, J = 3.2 Hz, C_{1''}), 131.6 (d, J = 8.1 Hz, 2C_{2''}-H_{p-fluorophenyl}), 130.8 (C₆-H), 126.8 (C₄-H), 126.2 (C_{4'''}-H), 125.9 (C_{3'''}-H), 123.9 (C_{5'''}-H), 123.3 (C₅-H, C₉), 121.4 (C_{2'''}-H), 117.8 (CN), 115.2 (d, J = 21.3 Hz, 2C_{3''}-H_{p-fluorophenyl}), 110.0 (C₇H), 78.7 (C₃/C_{2'}), 62.0 (C_{3'}), 56.9 (C₅-H₂), 46.5 (C₄-H), 35.4 (N₁-CH₃) ppm. Anal. Calcd for C₂₆H₁₉FN₄OS: C, 68.71; H, 4.21; N, 12.33. Found: C, 68.50; H, 4.35; N, 12.16.

(2',3',3',4',4',3')-(Benzo[d]thiazol-2-yl)-4'-(4-cyanophenyl)-1'-methyl-2-oxospiro[indoline-3,2'-pyrrolidine]-3'-carbonitrile (**5f**). Yield: 380 mg (65.9%) from 359 mg of **4f**; white crystals, mp 159–161 °C. ¹H NMR (CDCl₃, 600 MHz): δ 8.03 (d, J = 8.4 Hz, 1H, C_{5'''}-H), 7.99 (d, J = 7.2 Hz, 1H, C₄-H), 7.84 (d, J = 8.4 Hz, 2H, Ar-C_{2''}-H_{p-cyanophenyl}), 7.68 (d, J = 7.8 Hz, 1H, C_{2'''}-H), 7.63 (d, J = 8.4 Hz, 2H, Ar-C_{3''}-H_{p-cyanophenyl}), 7.53 (s, 1H, N₁-H), 7.45 (t, J = 7.2 Hz, 1H, C_{4'''}-H), 7.38 (t, J = 7.8 Hz, 1H, C₆-H), 7.36 (t, J = 7.2 Hz, 1H, C_{3'''}-H), 7.25 (t, J = 7.8 Hz, 1H, C₅-H), 6.73 (d, J = 7.8 Hz, 1H, C₇-H), 5.85 (dd, J = 10.8, 6.6 Hz, 1H, C₄-H), 3.91 (app t, J = 10.2 Hz, 1H, C₅-H_a), 3.78 (dd, J

= 9.6, 6.6 Hz, 1H, C₅-H_b), 2.25 (s, 3H, N₁-CH₃) ppm; ¹³C NMR (150 MHz, CDCl₃): δ 174.7 (q, C₂=O), 160.6 (q, C_{7'''}), 151.9 (q, C_{6'''}), 142.5 (q, C_{1''}), 142.0 (q, C₈), 135.5 (q, C_{1'''}), 132.1 (2C_{3''}-H_{p-cyanophenyl}), 131.1 (C₆H), 130.8 (2C_{2''}-H_{p-cyanophenyl}), 126.9 (C₄-H), 126.5 (C_{4'''}-H), 126.1 (C_{3'''}-H), 124.1 (C_{5'''}-H), 123.5 (C₅-H), 122.9 (q, C₉), 121.5 (C_{2'''}-H), 118.8 (Ar-C₅''-N), 117.5 (CN), 111.8 (ArC_{4'}-CN), 109.9 (C₇H), 78.6 (C₃/C_{2'}), 61.6 (C_{3'}), 56.5 (C₅-H₂), 46.7 (C₄-H), 35.5 (N₁-CH₃) ppm. Anal. Calcd for C₂₇H₁₉N₅OS: C, 70.26; H, 4.15; N, 15.17. Found: C, 70.59; H, 4.45; N, 15.01.

(2',3',3',4',4',3')-(Benzo[d]thiazol-2-yl)-4'-(4-cyanophenyl)-1'-methyl-2-oxospiro[indoline-3,2'-pyrrolidine]-3'-carbonitrile (**5f**). Yield: 175 mg (30.3%) from 359 mg of **4f**; pale yellow crystals, mp 150–152 °C. ¹H NMR (CDCl₃, 600 MHz): δ 8.75 (s, 1H, N₁-H), 8.14 (d, J = 7.8 Hz, 1H, C_{5'''}-H), 7.78 (d, J = 8.4 Hz, 2H, Ar-C_{2''}-H_{p-cyanophenyl}), 7.72 (d, J = 8.4 Hz, 1H, C_{2'''}-H), 7.64 (d, J = 8.4 Hz, 2H, Ar-C_{3''}-H_{p-cyanophenyl}), 7.53 (t, J = 7.8 Hz, 1H, C_{4'''}-H), 7.40 (t, J = 8.4 Hz, 1H, C_{3'''}-H), 7.09 (t, J = 7.2 Hz, 1H, C₆-H), 6.83 (d, J = 7.8 Hz, 1H, C₇-H), 6.57 (t, J = 7.8 Hz, 1H, C₅-H), 6.52 (d, J = 7.8 Hz, 1H, C₄-H), 5.56 (app t, J = 8.4 Hz, 1H, C₄-H), 4.25 (app t, J = 9.6 Hz, 1H, C₅-H_a), 3.68 (app t, J = 9.0 Hz, 1H, C₅-H_b), 2.32 (s, 3H, N₁-CH₃) ppm; ¹³C NMR (150 MHz, CDCl₃): δ 176.3 (q, C₂=O), 165.8 (q, C_{7'''}), 151.9 (q, C_{6'''}), 141.8 (q, C_{1''}), 141.3 (q, C₈), 135.5 (q, C_{1'''}), 132.3 (2C_{3''}-H_{p-cyanophenyl}), 130.7 (2C_{2''}-H_{p-cyanophenyl}), 130.4 (C₆-H), 126.7 (C_{4'''}-H), 126.1 (C_{3'''}-H), 126.0 (C₄-H), 123.8 (C_{5'''}-H), 123.4 (q, C₉), 122.7 (C₅-H), 121.6 (C_{2'''}-H), 118.6 (Ar-C₅''-N), 118.0 (CN), 112.1 (ArC_{4'}-CN), 110.6 (C₇-H), 80.1 (C₃/C_{2'}), 60.9 (C_{3'}), 57.2 (C₅-H₂), 51.4 (C₄-H), 35.5 (N₁-CH₃) ppm. Anal. Calcd for C₂₇H₁₉N₅OS: C, 70.26; H, 4.15; N, 15.17. Found: C, 70.43; H, 4.47; N, 15.09.

(2',3',3',4',4',3')-(Benzo[d]thiazol-2-yl)-1'-methyl-4'-(4-nitrophenyl)-2-oxospiro[indoline-3,2'-pyrrolidine]-3'-carbonitrile (**5g**). Yield: 460 mg (76.4%) from 384 mg of **4g**; orange crystals, mp 195–197 °C. ¹H NMR (CDCl₃, 600 MHz): δ 8.19 (d, J = 9.0 Hz, 2H, Ar-C_{3''}-H_{p-nitrophenyl}), 8.06 (d, J = 7.8 Hz, 1H, C_{5'''}-H), 8.00 (d, J = 7.8 Hz, 1H, C₄-H), 7.91 (d, J = 9.0 Hz, 2H, Ar-C_{2''}-H_{p-nitrophenyl}), 7.69 (d, J = 7.8 Hz, 1H, C_{2'''}-H), 7.47 (t, J = 7.8 Hz, 1H, C_{4'''}-H), 7.40 (t, J = 7.8 Hz, 1H, C₆-H), 7.38 (s, 1H, N₁-H), 7.37 (t, J = 7.8 Hz, 1H, C_{3'''}-H), 7.26 (t, J = 7.5 Hz, 1H, C₅-H), 6.73 (d, J = 7.8 Hz, 1H, C₇-H), 5.93 (dd, J = 10.2, 6.6 Hz, 1H, C₄-H), 3.94 (app t, J = 10.2 Hz, 1H, C₅-H_a), 3.82 (dd, J = 9.6, 6.6 Hz, 1H, C₅-H_b), 2.27 (s, 3H, N₁-CH₃) ppm; ¹³C NMR (150 MHz, CDCl₃): δ 174.5 (q, C₂=O), 160.5 (q, C_{7'''}), 151.9 (q, C_{6'''}), 147.6 (C_{4'}-NO₂), 144.6 (q, C_{1''}), 141.9 (q, C₈), 135.6 (q, C_{1'''}), 131.1 (C₆-H), 131.0 (2C_{2''}-H_{p-nitrophenyl}), 127.0 (C₄-H), 126.5 (C_{4'''}-H), 126.2 (C_{3'''}-H), 124.1 (C_{5'''}-H), 123.5 (C₅-H), 123.4 (2C_{3''}-H_{p-nitrophenyl}), 122.8 (q, C₉), 121.5 (C_{2'''}-H), 117.5 (CN), 109.9 (C₇-H), 78.6 (C₃/C_{2'}), 61.7 (C_{3'}), 56.6 (C₅-H₂), 46.4 (C₄-H), 35.5 (N₁-CH₃) ppm. Anal. Calcd for C₂₆H₁₉N₅O₃S: C, 64.85; H, 3.98; N, 14.54. Found: C, 65.09; H, 4.17; N, 14.43.

(2',3',3',4',4',3')-(Benzo[d]thiazol-2-yl)-1'-methyl-4'-(4-nitrophenyl)-2-oxospiro[indoline-3,2'-pyrrolidine]-3'-carbonitrile (**5g**). Yield: 60 mg (10%) from 384 mg of **4g**; pale brown crystals, mp 185–187 °C. ¹H NMR (CDCl₃, 600 MHz): δ 8.21 (d, J = 8.8 Hz, 2H, Ar-C_{3''}-H_{p-nitrophenyl}), 8.17 (d, J = 7.8 Hz, 1H, C_{5'''}-H), 8.07 (s, 1H, N₁-H), 7.82 (d, J = 8.4 Hz, 2H, Ar-C_{2''}-H_{p-nitrophenyl}), 7.74 (d, J = 7.8 Hz, 1H, C_{2'''}-H), 7.55 (t, J = 8.4 Hz, 1H, C_{4'''}-H), 7.42 (t, J = 8.4 Hz, 1H, C_{3'''}-H), 7.10 (t, J = 7.8 Hz, 1H, C₆-H), 6.81 (d, J = 7.8 Hz, 1H, C₇-H), 6.55 (t, J = 7.8 Hz, 1H, C₅-H), 6.45 (d, J = 7.8 Hz, 1H, C₄-H), 5.60 (dd, J = 9.6, 8.4 Hz, 1H, C₄-H), 4.28 (app t, J = 10.2 Hz, 1H, C₅-H_a), 3.70 (dd, J

= 9.6, 8.4 Hz, 1H, C₅-H_a), 2.32 (s, 3H, N₁-CH₃) ppm; ¹³C NMR (150 MHz, CDCl₃): δ 176.4 (q, C₂=O), 165.7 (q, C₇'), 151.8 (q, C₆'), 147.7 (C₄'-NO₂), 143.9 (q, C₁'), 141.4 (q, C₈), 135.5 (q, C₁'), 130.9 (2C₂'H_p-nitrophenyl), 130.5 (C₆-H), 126.7 (C₄'-H), 126.1 (C₃'-H), 126.0 (C₄-H), 123.8 (C₅'-H), 123.7 (C₅-H), 123.3 (q, C₉), 122.7 (2C₃'H_p-nitrophenyl), 121.6 (C₂'-H), 118.0 (CN), 110.7 (C₇-H), 80.1 (C₃/C₂'), 60.8 (C₃'), 57.3 (C₅-H₂), 51.1 (C₄'-H), 35.4 (N₁-CH₃) ppm. Anal. Calcd for C₂₆H₁₉N₅O₃S: C, 64.85; H, 3.98; N, 14.54. Found: C, 65.03; H, 4.27; N, 14.39.

■ ASSOCIATED CONTENT

Data Availability Statement

The data underlying this study are available in the published article and its [Supporting Information](#).

Supporting Information

The Supporting Information is available free of charge at <https://pubs.acs.org/doi/10.1021/acsomega.4c01552>.

Copies of ¹H, ¹³C{¹H}, ¹⁹F, ¹³C-DEPT 90/135, ¹H-¹H-COSY, ¹H-¹³C-HSQC, and ¹H-¹³C-HMBC NMR spectra for compounds **5a–c**, **5'c**, **5d–f**, **5'f**, **5g**, **5'g**, regio- and stereochemical assignment of *exo*-cycloadduct (**5g**), regio- and stereochemical assignment of *endo*-cycloadduct (**5'g**), optimized ground state energies of *E*-configurations and *Z*-configurations of dipole **3** and dipolarophiles **4a–g**, HOMO and LUMO orbitals at **5a** and **6a** transitions states, optimized coordinates for **5a**, **5(TS-I)**, **5'a**, **5(TS-II)**, **6a**, **6(TS-I)**, **6'a**, **6(TS-II)** (PDF)

■ AUTHOR INFORMATION

Corresponding Authors

Essam M. Hussein – Department of Chemistry, Faculty of Science, Umm Al-Qura University, 21955 Makkah, Saudi Arabia; Department of Chemistry, Faculty of Science, Assiut University, 71516 Assiut, Egypt; Email: amhfarghaly@uqu.edu.sa, essam.hussein78@yahoo.com

Saleh A. Ahmed – Department of Chemistry, Faculty of Science, Umm Al-Qura University, 21955 Makkah, Saudi Arabia; Department of Chemistry, Faculty of Science, Assiut University, 71516 Assiut, Egypt; orcid.org/0000-0002-2364-0380; Email: saahmed@uqu.edu.sa, saleh_63@hotmail.com

Authors

Ziad Moussa – Department of Chemistry, College of Science, United Arab Emirates University, Al Ain, United Arab Emirates; orcid.org/0000-0002-3365-0451

Jabir H. Al-Fahemi – Department of Chemistry, Faculty of Science, Umm Al-Qura University, 21955 Makkah, Saudi Arabia

Munirah M. Al-Rooqi – Department of Chemistry, Faculty of Science, Umm Al-Qura University, 21955 Makkah, Saudi Arabia

Rami J. Obaid – Department of Chemistry, Faculty of Science, Umm Al-Qura University, 21955 Makkah, Saudi Arabia

M. Shaheer Malik – Department of Chemistry, Faculty of Science, Umm Al-Qura University, 21955 Makkah, Saudi Arabia

Alaa S. Abd-El-Aziz – Qingdao Innovation and Development Center, Harbin Engineering University, Qingdao 266400, China

Complete contact information is available at:

<https://pubs.acs.org/doi/10.1021/acsomega.4c01552>

Notes

The authors declare no competing financial interest.

■ ACKNOWLEDGMENTS

Dr. Ziad Moussa is grateful to the United Arab Emirates University (UAEU) and to the Research Office for supporting the research developed in his laboratory and reported herein (UPAR grant code G00004605).

■ REFERENCES

- (1) (a) James, D. M.; Kunze, H. B.; Faulkner, D. J. Two new brominated tyrosine derivatives from the sponge *Druinella* (= *Psammaphysilla*) *purpurea*. *J. Nat. Prod.* **1991**, *54*, 1137–1140. (b) Zheng, Y.-J.; Tice, C. M. The utilization of spirocyclic scaffolds in novel drug discovery. *Expert Opin. Drug Discovery* **2016**, *11*, 831–834.
- (2) (a) Cordell, G. A. *The Alkaloids: Chemistry and Biology*; Academic: San Diego, 1998. (b) Cui, C.-B.; Kakeya, H.; Osada, H. Novel mammalian cell cycle inhibitors, spirotryprostatins A and B, produced by *Aspergillus fumigatus*, which inhibit mammalian cell cycle at G₂/M phase. *Tetrahedron* **1996**, *52*, 12651–12666. (c) Xue, J.; Zhang, Y.; Wang, X.-L.; Fun, H. K.; Xu, J. H. Photoinduced Reactions of 1-Acetylisatin with Phenylacetylenes. *Org. Lett.* **2000**, *2*, 2583–2586. (d) Klumpp, D. A.; Yeung, K. Y.; Prakash, G. K. S.; Olah, G. A. Preparation of 3, 3-diaryloxindoles by superacid-induced condensations of isatins and aromatics with a combinatorial approach. *J. Org. Chem.* **1998**, *63*, 4481–4484.
- (3) (a) Murugan, R.; Anbazhagan, S.; Sriman Narayanan, S. Synthesis and in vivo antidiabetic activity of novel dispiropyrrrolidines through [3 + 2] cycloaddition reactions with thiazolidinedione and rhodanine derivatives. *Eur. J. Med. Chem.* **2009**, *44*, 3272–3279. (b) Karthikeyan, K.; Senthil Kumar, R.; Muralidharan, D.; Perumal, P.T. Diastereoselective synthesis of pyrrolidines via 1, 3-dipolar cycloaddition of a chiral azomethine ylide. *Tetrahedron Lett.* **2009**, *50*, 7175–7179. (c) Girgis, A. S. Regioselective synthesis of dispiro[1*H*-indene-2,3'-pyrrolidine-2',3"-[3*H*]indole]-1,2''(1''*H*)-diones of potential anti-tumor properties. *Eur. J. Med. Chem.* **2009**, *44*, 91–100. (d) Ranjith Kumar, R.; Perumal, S.; Manju, S.C.; Bhatt, P.; Yogeewari, P.; Sriram, D. An atom economic synthesis and antitubercular evaluation of novel spiro-cyclohexanones. *Bioorg. Med. Chem. Lett.* **2009**, *19*, 3461–3465. (e) Aicher, T. D.; Knorr, D. C.; Smith, H. C. Synthesis of chiral tetrahydropyrrolo[2,1-*b*]thiazol-5(6*H*)-ones. *Tetrahedron Lett.* **1998**, *39*, 8579–8580. (f) Baldwin, J. E.; Freeman, R. T.; Lowe, C.; Schofield, C. J.; Lee, E. A γ -lactam analogue of the penems possessing antibacterial activity. *Tetrahedron* **1989**, *45*, 4537–4550. (g) Trapani, G.; Franco, M.; Latrofa, A.; Carotti, A.; Cellamare, S.; Serra, M.; Ghiani, C. A.; Tuligi, G.; Biggio, G.; Liso, G. Synthesis and Anticonvulsant Activity of Some 1,2,3,4-Tetrahydropyrrolo[2,1-*b*]benzothiazol-, -thiazol- or -oxazol-1-ones in Rodents. *J. Pharm. Pharmacol.* **2011**, *48*, 834–840.
- (4) Farag, A. A. Synthesis and antimicrobial activity of 5-(morpholinofulfonyl) isatin derivatives incorporating a thiazole moiety. *Drug Res.* **2015**, *65*, 373–379.
- (5) (a) Lu, Y.; Li, C.-M.; Wang, Z.; Ross, C. R.; Chen, J.; Dalton, J. T.; Li, W.; Miller, D. D. Discovery of 4-substituted methoxy benzoyl-aryl-thiazole as novel anticancer agents: synthesis biological evaluation and structure-activity relationships. *J. Med. Chem.* **2009**, *52*, 1701–1711. (b) Chandrappa, S.; Chandru, H.; Sharada, A. C.; Vinaya, K.; Ananda Kumar, C. S.; Thimmegowda, N. R.; Nagegowda, P.; Karuna Kumar, M.; Rangappa, K. S. Synthesis and in vivo anticancer and antiangiogenic effects of novel thioxothiazolidin-4-one derivatives against transplantable mouse tumor. *Med. Chem. Res.* **2010**, *19*, 236–249.
- (6) Satoh, A.; Nagatomi, Y.; Hirata, Y.; Ito, S.; Suzuki, G.; Kimura, T.; Maehara, S.; Hikichi, H.; Satow, A.; Hata, M.; Ohta, H.; Kawamoto, H. Discovery and in vitro and in vivo profiles of 4-fluoro-N-[4-[6-(isopropylamino)pyrimidin-4-yl]-1,3-thiazol-2-yl]-N-methylbenzamide as novel class of an orally active metabotropic glutamate receptor 1 antagonist. *Bioorg. Med. Chem.* **2009**, *19*, 5464–5468.
- (7) Sondhi, S. M.; Singh, N.; Lahoti, A. M.; Bajaj, K.; Kumar, A.; Lozach, O.; Meijer, L. Synthesis of acridinylthiazolino derivatives and

their evaluation for antiinflammatory analgesic and kinase inhibition activities. *Bioorg. Med. Chem.* **2005**, *13*, 4291–4299.

(8) (a) 3-Dipolar Cycloaddition Chemistry. Padwa, A., Ed.; Wiley/Interscience: New York, Vols. 1 and 2, 1984. (b) Poornachandran, M.; Raghunathan, R. Synthesis of Spirooxindolo/Spiroindano Nitro Pyrrolizidines through Regioselective Azomethine Ylide Cycloaddition Reaction. *Synth. Commun.* **2007**, *37*, 2507–2516. (c) El Moncef, A.; El Hadrami, E. M.; Ben-Tama, A.; de Arellano, C. R.; Zaballos-Garcia, E.; Stiriba, S. E. Synthesis and characterization of new 1,4 and 1,5-disubstituted glucopyranosyl 1,2,3-triazole by 1,3-dipolar cycloaddition. *J. Mol. Struct.* **2009**, *929*, 6–9. (d) Lakshmi, N. V.; Thirumurugan, P.; Perumal, P. T. An expedient approach for the synthesis of dispiropyrrrolidine bisoxindoles, spiropyrrrolidine oxindoles and spiroindane-1,3-diones through 1,3-dipolar cycloaddition reactions. *Tetrahedron Lett.* **2010**, *51*, 1064–1068.

(9) Domingo, L.; Rios-Gutierrez, M.; Perez, P. Applications of the conceptual density functional theory indices to organic chemistry reactivity. *Molecules* **2016**, *21*, 748.

(10) Nasri, L.; Rios-Gutiérrez, M.; Nacereddine, A. K.; Djerourou, A.; Domingo, L. R. A molecular electron density theory study of [3 + 2] cycloaddition reactions of chiral azomethine ylides with β -nitrostyrene. *Theor. Chem. Acc.* **2017**, *136*, 104.

(11) (a) Domingo, L. R.; Saez, J. A. Understanding the electronic reorganization along the nonpolar [3 + 2] cycloaddition reactions of carbonyl ylides. *J. Org. Chem.* **2011**, *76*, 373–379. (b) Domingo, L. R.; Rios-Gutiérrez, M.; Pérez, P. A molecular electron density theory study of the [3 + 2] cycloaddition reaction of nitrones with strained allenes. *RSC Adv.* **2017**, *7*, 26879–26887.

(12) Domingo, L. R.; Saéz, J. A.; Zaragoza, R. J.; Arnó, M. Understanding the participation of quadricyclane as nucleophile in polar [2 σ + 2 σ + 2 π] cycloadditions toward electrophilic π molecules. *J. Org. Chem.* **2008**, *73*, 8791–8799.

(13) (a) Hussein, E. M.; Abdel-Monem, M. I. Regioselective synthesis and anti-inflammatory activity of novel dispiro[pyrazolidine-4,3'-pyrrolidine-2',3''-indoline]-2'',3,5-triones. *Arkivoc* **2011**, *2011*, 85–98. (b) Hussein, E. M.; Ahmed, S. A.; Guesmi, N. E.; Khairou, K. S. 1,3-Dipolar cycloaddition approach to novel dispiro[pyrazolidine-4,3'-pyrrolidine-2',3''-indoline]-2'',3,5-triones. *J. Chem. Res.* **2017**, *41*, 346–351. (c) Hussein, E. M.; Ahmed, S. A.; Althagafi, I. I. A convenient regioselective synthesis of novel spirooxindolinopyrrolizidines incorporating the pyrene moiety through [3 + 2]-cycloaddition reaction. *Heterocycl. Commun.* **2017**, *23*, 379–384. (d) Hussein, E. M.; Moussa, Z.; Ahmed, S. A. Exclusive regioselective 1,3-dipolar cycloaddition of 9-diazo-9H-fluorene and diphenyldiazomethane to 2-arylideneindane-1,3-diones: new approach toward effective synthesis of novel spiroazole derivatives. *Monatsh. Chem.* **2018**, *149*, 2021–2030. (e) Hussein, E. M.; Moussa, Z.; El Guesmi, N.; Ahmed, S. A. Facile access to regio- and stereoselective synthesis of highly functionalized spiro[indoline-3,2'-pyrrolidines] incorporating a pyrene moiety: experimental, photophysical and theoretical approach. *RSC Adv.* **2018**, *8*, 24116–24127. (f) Hussein, E. M.; El Guesmi, N.; Moussa, Z.; Pal, U.; Pal, S. K.; Saha-Dasgupta, T.; Ahmed, S. A. Unprecedented regio- and stereoselective synthesis of pyrene-grafted dispiro[indoline-3,2'-pyrrolidine-3,3''-indolines]: expedient experimental and theoretical insights into polar [3 + 2] cycloaddition. *ACS Omega* **2020**, *5*, 24081–24094. (g) Hussein, E. M.; Moussa, Z.; Pal, U.; Alsantali, R. I.; Alzahrani, A. Y. A.; Obaid, R. J.; Alzahrani, F. M.; Al-Rooqi, M. M.; Alsharif, M. A.; El Guesmi, N.; Jassas, R. S.; Shaheer Malik, M.; Altass, H. M.; Pal, S. K.; Saha Dasgupta, T.; Ahmed, S. A. Regio- and stereoselectivity of the 1,3-dipolar cycloaddition of azomethine ylides to (E)-3-(2-oxo-2-(pyren-1-yl)ethylidene)indolin-2-ones: A combined experimental and theoretical study. *Arab. J. Chem.* **2022**, *15*, 103855. (h) Hussein, E. M.; El Guesmi, N.; Maji, T. K.; Jassas, R. S.; Alsimaree, A. A.; Altass, H. M.; Moussa, Z.; Pal, S. K.; Ahmed, S. A. Synthesis and photophysical properties of benzimidazoles grafted pyrazole-containing pyrene or fluorene moiety: A combined spectroscopic and computational study. *J. Photochem. Photobiol. A: Chem.* **2021**, *419*, 113465.

(14) Fukui, K. Recognition of stereochemical paths by orbital interaction. *Acc. Chem. Res.* **1971**, *4*, 57–64.

(15) Sustmann, R. Orbital energy control of cycloaddition reactivity. *Pure Appl. Chem.* **1974**, *40*, 569–593.

(16) Parr, R. G.; Yang, W. *Density Functional Theory of Atoms and Molecules*; Oxford University Press: Oxford, 1989.

(17) (a) Geerlings, P.; De Proft, F.; Langenaeker, W. Conceptual density functional theory. *Chem. Rev.* **2003**, *103*, 1793–1873. (b) Chermette, H. Chemical reactivity indexes in density functional theory. *J. Comput. Chem.* **1999**, *20*, 129–154.

(18) Domingo, L. R.; Rios-Gutierrez, M.; Pérez, P. Applications of the conceptual density functional theory indices to organic chemistry reactivity. *Molecules* **2016**, *21*, 748.

(19) Pérez, P.; Domingo, L. R.; Aizman, A.; Contreras, R. *Theoretical Aspects of Chemical Reactivity*; Toro-Labbé, A., Ed.; Elsevier: Amsterdam, 2006; pp 167–238.

(20) Perez, P.; Domingo, L. R.; Jose Aurell, M.; Contreras, R. Quantitative characterization of the global electrophilicity pattern of some reagents involved in 1,3-dipolar cycloaddition reactions. *Tetrahedron* **2003**, *59*, 3117–3125.

(21) Parr, R. G.; Donnelly, R. A.; Levy, M.; Palke, W. E. Electronegativity: the density functional viewpoint. *J. Chem. Phys.* **1978**, *68*, 3801–3807.

(22) Parr, R. G.; Pearson, R. G. Absolute hardness: companion parameter to absolute electronegativity. *J. Am. Chem. Soc.* **1983**, *105*, 7512–7516.

(23) (a) Liu, S. B. Electrophilicity. In *Chemical reactivity theory: A density functional view*; Chattaraj, P. K., Ed.; Taylor and Francis, 2009; p 179. (b) Gonzalez, M. M.; Cardenas, C.; Rodriguez, J. I.; Liu, S. B.; Heidar-Zadeh, F.; Miranda-Quintana, R. A.; Ayers, P. W. Quantitative Electrophilicity Measures. *Acta Phys.-Chim. Sin.* **2018**, *34*, 662–674. (c) Parr, R. G.; Szentpaly, L. v.; Liu, S. Electrophilicity Index. *J. Am. Chem. Soc.* **1999**, *121*, 1922–1924.

(24) (a) Domingo, L. R.; Aurell, M. J.; Pérez, P.; Contreras, R. Quantitative characterization of the global electrophilicity power of common diene/dienophile pairs in Diels–Alder reactions. *Tetrahedron* **2002**, *58*, 4417–4423. (b) Rios-Gutierrez, M.; Saz Sousa, A.; Domingo, L. R. Electrophilicity and nucleophilicity scales at different DFT computational levels. *J. Phys. Org. Chem.* **2023**, *36*, No. e4503.

(25) Gázquez, J. L.; Cedillo, A.; Vela, A. Electrodonating and electroaccepting powers. *J. Phys. Chem. A* **2007**, *111*, 1966–1970.

(26) Kohn, W.; Sham, L. Self-consistent equations including exchange and correlation effects. *J. Phys. Rev.* **1965**, *140*, A1133–A1138.

(27) Chattaraj, P. K.; Maiti, B. Reactivity dynamics in atom–field interactions: a quantum fluid density functional study. *J. Phys. Chem. A* **2001**, *105*, 169–183.

(28) Jaramillo, P.; Pérez, P.; Contreras, R.; Tiznado, W.; Fuentealba, P. Definition of a nucleophilicity scale. *J. Phys. Chem. A* **2006**, *110*, 8181–8187.

(29) Domingo, L. R.; Arno, M.; Contreras, R.; Pérez, P. Density functional theory study for the cycloaddition of 1,3-butadienes with dimethyl acetylenedicarboxylate. Polar stepwise vs concerted mechanisms. *J. Phys. Chem. A* **2002**, *106*, 952–961.

(30) Pratihari, S.; Roy, S. Nucleophilicity and site selectivity of commonly used arenes and heteroarenes. *J. Org. Chem.* **2010**, *75*, 4957–4963.

(31) Pratihari, S.; Roy, S. Correction to nucleophilicity and site selectivity of commonly used arenes and heteroarenes. *J. Org. Chem.* **2011**, *76*, 4219.

(32) (a) Pérez, P.; Toro-Labbé, A.; Aizman, A.; Contreras, R. Comparison between experimental and theoretical scales of electrophilicity in benzhydryl cations. *J. Org. Chem.* **2002**, *67*, 4747–4752. (b) Domingo, L. R.; Aurell, M. J.; Perez, P.; Contreras, R. Quantitative characterization of the local electrophilicity of organic molecules. understanding the regioselectivity on Diels–Alder Reactions. *J. Phys. Chem. A* **2002**, *106*, 6871–6875. (c) Chattaraj, P. K.; Maiti, B.; Sarkar, U. Philicity: A unified treatment of chemical reactivity and selectivity. *J. Phys. Chem. A* **2003**, *107*, 4973–4975. (d) Domingo, L. R.; Pérez, P.; Sáez, J. A. Understanding the local reactivity in polar organic reactions through electrophilic and nucleophilic Parr functions. *RSC Adv.* **2013**, *3*, 1486–1494.

(33) Chattaraj, P. K.; Duley, S.; Domingo, L. R. Understanding local electrophilicity/ nucleophilicity activation through a single reactivity difference index. *Org. Biomol. Chem.* **2012**, *10*, 2855–2861.

(34) (a) Chattaraj, P. K.; Lee, H.; Parr, R. G. HSAB principle. *J. Am. Chem. Soc.* **1991**, *113*, 1855–1856. (b) Ayers, P. W. The physical basis of the hard/soft acid/base principle. *Faraday Discuss. R. Chem. Soc.* **2007**, *135*, 161–190. (c) Pearson, R. G. Hard and soft acids and bases. *J. Am. Chem. Soc.* **1963**, *85*, 3533–3539.

(35) Nguyen, L. T.; Proft, F. D.; Chandra, A. K.; Uchimaru, T.; Nguyen, M. T.; Geerlings, P. Nitrous oxide as a 1,3-dipole: A theoretical study of its cycloaddition mechanism. *J. Org. Chem.* **2001**, *66*, 6096–6103.

(36) Yang, W. T.; Parr, R. G. Hardness, softness, and the Fukui function in the electron theory of metals and catalysis. *Proc. Natl. Acad. Sci. U. S. A.* **1985**, *82*, 6723–6726.

(37) Lu, T.; Chen, F. Quantitative analysis of molecular surface based on improved Marching Tetrahedra algorithm. *J. Mol. Graph. Model.* **2012**, *38*, 314–323.

(38) (a) Hayden, A. E.; DeChancie, J.; George, A. H.; Dai, M.; Yu, M.; Danishefsky, S. J.; Houk, K. N. Origins of the Regioselectivities in the Diels-Alder Reactions of Vinylindenes with 1,4-Quinone Monoketal and Acrolein Dienophiles. *J. Org. Chem.* **2009**, *74*, 6770–6776. (b) Murray, J. S.; Yepes, D.; Jaque, P.; Politzer, P. Insights into some Diels-Alder cycloadditions via the electrostatic potential and the reaction force constant. *Comput. Theor. Chem.* **2015**, *1053*, 270–280. (c) Soleymani, M. A density functional theory study on the [3 + 2] cycloaddition of *N*-(*p*-methylphenacyl)benzothiazolium ylide and 1-nitro-2-(*p*-methoxyphenyl) ethene: the formation of two diastereomeric adducts via two different mechanisms. *Theor. Chem. Acc.* **2019**, *138*, 87.

(39) (a) Benchouk, W.; Mekelleche, S. M.; Aurell, M. J.; Domingo, L. R. Understanding the regio- and chemoselective polar [3 + 2] cycloaddition of the Padwa carbonyl ylides with α -methylene ketones. A DFT study. *Tetrahedron* **2009**, *65*, 4644–4651. (b) Bentabed-Ababsa, G.; Derdour, A.; Roisnel, T.; Saez, J. A.; Perez, P.; Chamorro, E.; Domingo, L. R.; Mongin, F. A Combined Experimental and Theoretical Study of the Polar [3 + 2] Cycloaddition of Electrophilically Activated Carbonyl Ylides with Aldehydes and Imines. *J. Org. Chem.* **2009**, *74*, 2120–2133.

(40) Domingo, L. R. A new C–C bond formation model based on the quantum chemical topology of electron density. *RSC Adv.* **2014**, *4*, 32415–32428.

(41) Shirani, M. A.; Maleki, M. H.; Asadi, P.; Dinari, M. Benzothiazolopyridine compounds: Facial synthesis, characterization, and molecular docking study on estrogen and progesterone receptors. *J. Mol. Struct.* **2021**, *1243*, 130792.

(42) (a) Miehlich, B.; Savin, A.; Stoll, H.; Preuss, H. Results obtained with the correlation energy density functionals of Becke and Lee, Yang and Parr. *Chem. Phys. Lett.* **1989**, *157*, 200–206. (b) Becke, A. D. Density-functional thermochemistry. III. The role of exact exchange. *J. Chem. Phys.* **1993**, *98*, 5648–5652.

(43) (a) Reed, A. E.; Curtiss, L. A.; Weinhold, F. Intermolecular interactions from a natural bond orbital, donor-acceptor viewpoint. *Chem. Rev.* **1988**, *88*, 899–926. (b) Contreras, R.; Fuentealba, P.; Galván, M.; Pérez, P. A direct evaluation of regional Fukui functions in molecules. *Chem. Phys. Lett.* **1999**, *304*, 405–413.